Physics – Uspekhi **52** (12) 1193 – 1212 (2009)

REVIEWS OF TOPICAL PROBLEMS PACS numbers: **71.38. – k**, **74.20. – z**, **74.72. – h**

Electron–phonon coupling in underdoped high-temperature superconductors

A S Mishchenko

DOI: 10.3367/UFNe.0179.200912b.1259

Contents

Abstract. Results indicating the important role of the electron – phonon coupling in high-temperature superconductivity compounds are presented, with emphasis on its implications for angle-resolved photoemission and optical conductivity. The dimensionless phonon coupling constant λ is determined by comparing the experimental and theoretical results. Although undoped materials are in the strong-coupling ($\lambda \sim 1$) regime, hole doping decreases λ, bringing compounds to the intermediate-coupling regime at optimum hole concentrations.

1. Introduction

For many years, the discussion on the role of the electron–phonon coupling (EPC) in the physics of high-temperature superconductivity (HTSC), set up at once after the discovery of HTSC, has split opponents into several competing groups, all seemingly speaking different languages with no communication with each other because of the reluctance to follow, or at least consider, the arguments of opponents. The variety of opinions ranges from the complete negation of the role of EPC in the physics of HTSC [1, 2] to the statement that the binding energy of the polaron is an order of magnitude larger than any characteristic energy of the magnetic subsystem, and therefore just the magnetic system is irrelevant [3, 4]. Both of the above radical statements have been criticized many times. For example, the results of numerous calculations [5–9] give grounds to disagree [10, 11] with the total negation of the role of EPC. On the other hand, the success of the extended $t-J$ model in describing the peak observed in the angle-resolved photoemission spectra (ARPES) [12, 13] does not allow disregarding the role of the magnetic subsystem completely. Correspondingly, there is an opinion that interactions with both magnetic and lattice subsystems are important [14].

Even very recently, in addressing the problem based only on the spectroscopy of HTSC compounds, it seemed that the data indicate a minor effect of EPC on the ARPES and optical absorption. First, dispersion observed in the ARPES peak well agrees with the predictions of the extended $t-t'-t''-J$ model [12] describing the movement of a hole in an antiferrromagnet [13, 15, 16]. Second, the results of calculations of optical absorption in the framework of the $t-J$ model predicted a peak at approximately the energy [17–30] of the mid-infrared (MIR) absorption band observed in experiment [31–36].

Seeming agreement between experiment and the interpretation of spectroscopy of HTSC compounds in terms of the pure $t-t'-t''-J$ model was destroyed by a new generation of experimental and theoretical methods over a few years. On the one hand, reaching a few meV resolution with the ARPES technique [12] and the significant achieve-

A S Mishchenko Cross-Correlated Materials Research Group (CMRG), ASI, RIKEN, Wako, Saitama 351-0198, Japan
Tel. (81-48) 462 11 11, ext. 63 62. Fax (81-48) 462 47 03
E-mail: mishchenko@riken.jp
Russian Research Centre 'Kurchatov Institute'
pl. Kurchatova 1, 123182 Moscow, Russian Federation
Tel. (7-499) 196 91 48. Fax (7-499) 943 00 74

Received 21 May 2009, revised 2 July 2009
Uspekhi Fizicheskikh Nauk **179** (12) 1259 – 1280 (2009)
DOI: 10.3367/UFNr.0179.200912b.1259
Translated by A S Mishchenko; edited by A M Semikhatov

ments of the ellipsometry technique to measure optical absorption avoiding the Kramers–Kronig transformation [37, 38] have enabled experimentalists to study the fine structure of spectra. On the other hand, two methods developed during the last decade, the diagrammatic Monte Carlo (DMC) method in imaginary time [39–62] and the stochastic optimization method for analytic continuation from imaginary time to real frequencies [41, 50, 51, 60–63], have given the means to calculate spectra of systems with complex Hamiltonians without significant approximations.

The puzzle concerning the linewidth of ARPES in undoped HTSC compounds became the first major contradiction that destroyed harmony based on the agreement between experimental data at low resolution and the results of approximate theoretical calculations. The peak in ARPES, obtained in the *exact solution* of the $t-J$ model [44], appeared to be narrow, whereas the linewidth observed in experiment was much larger than the experimental resolution. The experimental linewidth is so large that the dispersion bandwidth is sometimes less than the peak width [64].

A natural extension of the model with a hole in an antiferromagnet is the introduction of EPC, whose role in the physics of HTSC compounds was recently demonstrated in various experiments. At a first glance, a good description of the experimental dispersion of the ARPES peak in the framework of the extended $t-t'-t''-J$ model was a serious argument against the EPC because, as it seemed, significant EPC has to change the dispersion beyond recognition. However, as was shown by exact calculations, inclusion of a strong EPC is capable of reproducing the situation observed in experiment. The real particle, which is a strong-coupling polaron with an almost zero dispersion, has a very small weight and cannot be discerned in experimental spectra [49]. At the same time, a broad Franck–Condon shake-off peak with a large weight is separated in energy from the dispersionless polaron and exactly copies the dispersion of a particle that is not coupled to phonons [49, 65].

The conclusion about the important role of both the lattice and magnetic subsystems in the formation of the spectral response, drawn from the analysis of ARPES, was confirmed by further experimental and theoretical studies. The existence of polarons in undoped HTSC compounds was confirmed by ARPES measurements [66]. Optical absorption spectra obtained by ellipsometry revealed two peaks instead of one in the MIR region of weakly doped HTSC compounds [57]. The above structure of the optical absorption spectra is well reproduced in the framework of the $t-t'-t''-J$ model when the EPC is taken into account. Another confirmation of the conclusion follows from the analysis of the temperature dependence of the linewidth of ARPES peaks, which cannot be explained either by purely magnetic models or by entirely polaronic ones [67]. However, the interplay between magnetic and lattice degrees of freedom allows describing the observed situation [56].

Estimates of the EPC strength in the framework of the model where the Zang–Rice singlet is coupled to phonons, as well as from the measurement of the energy difference between the polaron state and the Franck–Condon peak, led to a $\lambda \approx 1$ value of the dimensionless coupling constant in undoped compounds [68, 69], which corresponds to the strong-coupling regime in the $t-t'-t''-J$ model. However, the EPC strength rapidly decreases as the doping level increases [57, 70] and the EPC reaches the intermediate-coupling regime at optimal doping levels.

Because of the enormous interest in HTSC, there are many reviews examining various aspects of the physics of HTSC [5, 12, 14, 30, 32, 71–85].

2. Models describing the magnetic subsystem and the electron–phonon coupling

It is well known that the ground state of an undoped HTSC is an antiferromagnet whose doping by holes leads to the phase showing high temperatures of the superconducting transition. The extended $t-t'-t''-J$-H model, where a hole in a two-dimensional antiferromagnet is simultaneously magnetic and a lattice polaron that moves through the lattice emitting and absorbing magnons and phonons, is used in many papers in calculating the spectral properties of underdoped HTSC compounds.

In the spin-wave approximation of the $t-t'-t''-J$ model, a hole with the dispersion

$$\varepsilon(\mathbf{k}) = 4t' \cos(k_x)\cos(k_y) + 2t''\left[\cos(2k_x) + \cos(2k_y)\right] \quad (1)$$

moves in the magnon field

$$\hat{H}^0_{t-J} = \sum_{\mathbf{k}} \varepsilon(\mathbf{k}) h^\dagger_{\mathbf{k}} h_{\mathbf{k}} + \sum_{\mathbf{k}} \omega_{\mathbf{k}} \alpha^\dagger_{\mathbf{k}} \alpha_{\mathbf{k}} \,. \quad (2)$$

The dispersion of magnons is $\omega_{\mathbf{k}} = 2J(1-\gamma^2_{\mathbf{k}})^{1/2}$, where $\gamma_{\mathbf{k}} = (\cos k_x + \cos k_y)/2$. Here, $h_{\mathbf{k}}$ is the annihilation operator of the hole and $\alpha_{\mathbf{k}}$ is the annihilation operator of the magnon. The hole is scattered by magnons,

$$\hat{H}^{\mathrm{h-m}}_{t-J} = N^{-1/2} \sum_{\mathbf{k},\mathbf{q}} M_{\mathbf{k},\mathbf{q}} \left[h^\dagger_{\mathbf{k}} h_{\mathbf{k}-\mathbf{q}} \alpha_{\mathbf{k}} + \mathrm{h.c.}\right], \quad (3)$$

where $M_{\mathbf{k},\mathbf{q}}$ is the scattering vertex. The parameters t, t', and t'' are the amplitudes of the nearest, next-to-nearest, and next-next-to-nearest neighbor hopping. The Hamiltonian in (2), (3) corresponds to the $t-J$ model when the amplitudes t' and t'' are equal to zero and the hole that decouples from magnons has no dispersion. For a hole-doped (electron-doped) compound, $t > 0$, $t' < 0$, $t'' > 0$ ($t < 0$, $t' > 0$, $t'' < 0$) [86–89]. A detailed study of the spectral properties of the extended $t-t'-t''-J$ model is presented in Ref. [86].

A short-range EPC in the $t-t'-t''-J$-H model, where phonons are dispersionless with a frequency Ω_0, $\hat{H}^{\mathrm{ph}} = \Omega_0 \sum_{\mathbf{k}} b^\dagger_{\mathbf{k}} b_{\mathbf{k}}$, is defined by the Holstein Hamiltonian

$$\hat{H}^{\mathrm{e-ph}} = N^{-1/2} \sum_{\mathbf{k},\mathbf{q}} \frac{\sigma}{\sqrt{2M\Omega_0}} \left(h^\dagger_{\mathbf{k}} h_{\mathbf{k}-\mathbf{q}} b_{\mathbf{q}} + \mathrm{h.c.}\right). \quad (4)$$

Here, σ is the coupling constant, which is independent of the momentum or mass of the isotope, M is the mass of ions participating in lattice vibrations, and Ω_0 is the frequency of dispersionless phonons. The coefficient in front of the parentheses in the right-hand site of (4) is the standard coupling constant $\gamma = \sigma/\sqrt{2M\Omega_0}$ of the Holstein model. Hereafter, the EPC strength is characterized by the dimensionless coupling constant $\lambda = \gamma^2/(4t\Omega_0)$. The coupling constant $g = \gamma/\Omega_0$ is also used often. We note that if the interaction with magnetic subsystem (3) is neglected and the dispersion of the hole is taken to be $\varepsilon(\mathbf{k}) = 2t(\cos k_x + \cos k_y)$, then models (2) and (4) correspond to the standard Holstein model where a hole with the nearest-neighbor hopping t is locally coupled to dispersionless phonons.

In the framework of the $t-J$-H Hamiltonian, which is obtained by a reduction of the model describing real HTSC compounds, the scattering vertices on magnons $M_{\mathbf{k},\mathbf{q}}$ and phonons γ are abstract constants. The origin of EPC and an estimate of λ follow from a consideration of lattice dynamics in the framework of the three-band model and reduction of its Hamiltonian to the Hamiltonian in (3) and (4).

2.1 Reduction of the three-band model

The three-band model [90] includes one $3d_{x^2-y^2}$ orbital of copper (Cu) and two p orbitals of oxygen (O) in the CuO_2 plain. The Hamiltonian

$$\hat{H}_{3B} = \varepsilon_O \sum_{i\boldsymbol{\delta}\sigma} a^\dagger_{i\boldsymbol{\delta}\sigma} a_{i\boldsymbol{\delta}\sigma} + \varepsilon_d \sum_{i\sigma} c^\dagger_{i\sigma} c_{i\sigma} + U \sum_i n_{i\uparrow} n_{i\downarrow} + t_{pd} \sum_{i\boldsymbol{\delta}\sigma} P_{\boldsymbol{\delta}} (c^\dagger_{i\sigma} a_{i\boldsymbol{\delta}\sigma} + \text{h.c.}) \quad (5)$$

includes a term with the Coulomb repulsion U in the Cu orbital and terms describing hopping between Cu and O with the amplitude t_{pd}. The vector $\boldsymbol{\delta}$ defines the oxygen position in the unit cell and takes the values $(a/2, 0)$ and $(0, a/2)$ in the first term and $(\pm a/2, 0)$ and $(0, \pm a/2)$ in the last term. The $a^\dagger_{i\boldsymbol{\delta}\sigma}$ and $c^\dagger_{i\sigma}$ are the respective creation operators of an electron with spin σ at the ith atom of oxygen whose position is determined by $\boldsymbol{\delta}$ and at the ith copper ion. The energy ε_d (ε_O) corresponds to Cu (O) orbitals.

The above model is reduced to the $t-J$ model, where site i corresponds to the location of the copper ion. In the undoped system, every copper ion is in the d^9 configuration and each site is occupied by one hole. Most of the doped holes occupy oxygen orbitals and form a Zhang–Rice singlet [91] with a hole at the copper ion. This singlet is a hole in the $t-J$ model Hamiltonian

$$\hat{H}_{t-J} = -t \sum_{\langle ij\rangle,\sigma} (\tilde{c}^\dagger_{i\sigma} \tilde{c}_{j\sigma} + \text{h.c.}) + J \sum_{\langle ij\rangle} \left(S_i S_j + \frac{n_i n_j}{4} \right), \quad (6)$$

where $\tilde{c}_{j\sigma}$ is the projected (to avoid double occupancy) fermion annihilation operator, n_i is the number operator at the site i ($n_i < 2$), S_i is the spin-1/2 operator, J is the exchange integral, and $\langle ij\rangle$ denotes nearest neighbors in a two-dimensional lattice. Expressing spin operators in terms of spin waves and making Fourier and Bogoliubov transformations yields the spin-wave Hamiltonian (corresponding to (2) with $t' = 0$ and $t'' = 0$) [30, 92–96]. Model (2), which reproduces the experimental ARPES dispersion [13, 15, 16, 86, 97–100], is obtained when the hopping integrals t' and t'' to next-nearest neighbors are taken into account.

We note that the $t-J$ model can also be obtained from the Hubbard model [71]

$$H_H = -t \sum_{\langle ij\rangle,\sigma} (\tilde{c}^\dagger_{i\sigma} \tilde{c}_{j\sigma} + \text{h.c.}) + U \sum_i n_{i\uparrow} n_{i\downarrow}. \quad (7)$$

To study the interplay of magnetic correlations and EPC, the relatively simpler Hubbard model is usually chosen from two prototypical Hamiltonians (5) and (7).

2.2 Sources of the electron–phonon coupling in high-temperature superconductors

The reason for a strong EPC in strongly correlated systems such as HTSC compounds is the huge energy involved in the formation of the Zhang–Rice singlet. This energy of several eVs is a trivial constant for a rigid crystal lattice and fixed doping. But the phonon-induced lattice distortion changes the hopping integrals t_{pd} and leads to a strong EPC [68, 101–112]. Calculations in the framework of the shell model [113] with the EPC constants obtained from the three-band model led to the conclusion that the dispersionless constant is of the order of unity, $\lambda \sim 1$ [69]. The same value is obtained from the estimate of λ using the shift of the wide Franck–Condon ARPES peak with respect to the chemical potential [69].

Another important source of EPC is the strong long-range Fröhlich interaction with phonons polarized along the c-axis. Some of those phonons soften and broaden with doping [114, 115]. The importance of those phonons was noted long ago and the interaction of a polaron with lattice vibrations of such a type was studied in [117] by the Monte Carlo method [116]. Interest in the problem of coupling to such phonons, invoked by high-precision ARPES results in doped $Bi_2Sr_2CuO_6$ [119], was renewed recently [118].

We note that the large value of the coupling constant λ in HTSC compounds is caused by strong electron correlations because estimates of the EPC strength by the local density functional (LDA) method [120, 121] lead to an order of magnitude smaller value of λ [72]. However, these results are not reliable because the phonon linewidth [122] obtained in the framework of the LDA method, is an order of magnitude smaller than that observed in experiment [123]. Recent paper [124] contains the statement that phonons have little influence on photoemission spectra, and hence a kink in ARPES cannot be caused by EPC. However, as was later shown in [125], calculations by the density functional method [124] do not reproduce the dispersion or the linewidth of phonons either [126–130], and hence the applicability of these results to the description of electron dispersion is also doubtful. On the other hand, the strong EPC drawn from strong-correlation physics properly describes the phonon linewidth [68, 108]. A more detailed discussion of the various models and types of EPC in HTSC can be found in review [14].

3. Experimental evidence of the role of the electron–phonon coupling

Due to tremendous efforts applied to development of a theory of HTSC compounds, many particular properties of these compounds can be explained in the framework of different numerous models once the contradictions with other experimental facts are ignored. For example, the authors of Ref. [131] seek an explanation of the checkerboard structure in a set of more than ten predicted phases of various natures. Hence, given the many contradictory interpretations, the only unambiguous proof of the existence of a considerable EPC is given by the anomalies of phonon spectra and the isotope effect.

To determine which phonons are anomalous, a fit of the measured phonon spectrum is attempted using data of calculations in the framework of the shell model. Phonons with the energies considerably smaller that those predicted by the shell model are considered to be anomalous (see Refs [132–134]). For example, breathing and half-breathing phonons are anomalous in doped systems [114, 123, 130, 135–141]. Another property indicating that a phonon is anomalous is its large linewidth, sometimes reaching 5 meV [123], distinguishing the anomalous phonon from the normal ones, whose linewidth is set by experimental resolution. For

example, breathing and half-breathing phonons, strongly coupled to a Zhang–Rice singlet, have a large linewidth, whereas quadrupolar ones, having no coupling to the singlet, are narrow [130]. The O_Z^Z phonon associated with the movement of oxygen perpendicular to the CuO_2 plain has a very large linewidth (16 meV) [80, 114]. One more anomalous phonon is B_{1g}, changing its energy and linewidth with temperature [142–146]. A phonon anomaly at the wave vector $\mathbf{q} = (0.25, 0, 0)$, having a strong connection with charge distribution inhomogeneities, is also detected [126]. Studies of phonon spectra are extensively reviewed in [82].

The manifestation of the isotope effect in any of the electronic properties unambiguously points to the existence of the EPC. The long history of the study of the isotope effect shows that the effect in the superconducting phase considerably depends on the doping level; the effect vanishes at the optimal doping and increases as the doping decreases [147–159]. The effect is especially strong on the border separating the superconducting, antiferromagnetic, and spin-glass phases [160]. In addition to the influence, revealed in the above papers, of isotope substitution on the superconducting temperature, superfluid density, and effective mass of the carrier, an influence of isotope substitution on antiferromagnetic [161] and spin-glass [162] transitions is found. The strong influence of isotope substitution on the pseudogap formation temperature is reported in Refs [163–166]. Isotope substitution induced a shift of the peak in the infrared part of optical absorption spectra, interpreted as a two-magnon one-phonon transition in undoped compounds [167, 168], was observed in $YBa_2Cu_3O_6$ [169]. Studies of the influence of isotope substitution on optical absorption spectra have revealed that residual nonsubstituted O^{16} ions in the O^{18} matrix lead to the appearance of impurity-associated modes at low energies [170]. The influence of isotopic substitution on ARPES spectra is considered in Section 4.4 in detail.

In addition to the proof of the importance of EPC obtained by classical approaches, an additional proof was found in experimental studies of the time evolution of lattice deformation following a polar excitation of carriers [171]. Rearrangement of the lattice in these experiments was studied by the method of time-resolved electron diffraction. Tunnel experiments also show [172] that the tunnel current has peculiarities at the energy values corresponding to peaks of Raman scattering [173, 174], also evidencing considerable EPC. The same evidence can be found in the data of a recent experiment where an anomalously large photoinduced expansion in cuprates was observed [175].

4. Manifestations of the electron–phonon coupling in spectroscopy

As noted in the Introduction, one of the main contradictions between the theoretical description and experimental ARPES data in undoped compounds was the anomalous linewidth of the signal observed in ARPES. The experimental ARPES signal corresponds to the spectral function [Lehmann function (LF)] of one hole in the extended $t-t'-t''-J$ model in Eqns (2) and (3). The spectral function of this model [13, 44, 97] consists of a narrow resonance at low energies and an incoherent high-energy continuum. We note that in contrast to one-dimensional systems, where spin–charge separation is observed [176, 177], spin and charge do not separate in two-dimensional systems, and the weight (Z factor) of the ground state is not equal to zero [44, 178, 179]. Energy dispersion of this resonance, i.e., the dependence of energy on the wave vector, perfectly reproduced the experimentally observed dispersion of the peak. However, the experimentally observed peak linewidth at the wave vector $(\pi/2, \pi/2)$, corresponding to the lowest point of dispersion in energy, is larger than the whole bandwidth of dispersion [64, 66]. On the other hand, an exact solution of the $t-J$ model obtained by the DMC method shows that the theoretical peak linewidth in the ground state at the wave vector $(\pi/2, \pi/2)$ is negligibly small [44].

Early attempts to explain the anomalous linewidth by a coupling to additional bosonic excitations, e.g., phonons [180], faced the general question: is a situation possible, in principle, where the lifetime of a quasiparticle decreases by several orders of magnitude while dispersion is absolutely left intact? The explanation of line broadening due to imperfections of a crystal lattice must be discarded because doping induces further disorder, while the ARPES peak, on the contrary, becomes narrower with an increase in the doping level.

The first spectral manifestations of EPC were found in phonon spectra where phonon softening and line broadening were observed. The results of various theoretical approaches to the description of phonon anomalies of HTSC compounds are considered in Section 4.1.

The problem of the LF in the $t-J$-H model was solved in Ref. [49] and is discussed in Section 4.2. It turned out that already at relatively small EPC constants $\lambda > 0.4$, the situation resembles the experimental one. A real quasiparticle turns into an almost dispersionless small-radius polaron, which is not seen in ARPES because of its low weight. In contrast, the wide Franck–Condon shake-off peak inherits the dispersion of a quasiparticle of the $t-J$ model, uncoupled to phonons.

To reach agreement with the experimental situation, we must set $\lambda > 0.4-0.55$ in the $t-J$-H model [49, 181], although in the more realistic $t-t'-t''-J$ model, the condition $\lambda > 0.6$ must be satisfied [52]. Hence, a crucial request to determine the value of the dimensionless EPC coupling constant λ was put forward. The problem was solved by different methods [69]. Estimates for λ obtained from data on the change in the Zhang–Rice singlet energy under lattice deformation by phonons, from the measured linewidth, and from the shift of the ARPES peak relative to the chemical potential, resulted in the same value $\lambda \sim 1$, which is sufficiently large to accomplish the scenario suggested in Ref. [49]. Different methods of obtaining an estimate for the EPC coupling constant are described in Section 4.3.

Naturally, a decisive experiment is needed to interpret ARPES data in the framework of strong-coupling polarons. This can be an experiment studying the influence of isotope substitution on ARPES. Theoretical studies of the isotope effect on the ARPES of undoped compounds were performed in Ref. [52] (see Section 4.4). Studies of the isotope effect in optimally doped compounds passed through several controversial stages [183–185] before reliable results were found in [182]. Studies of the isotope effect in undoped compounds are even more difficult, and hence experimental verification of the predictions made in Ref. [52] has not been done yet.

It was noted in early work on ARPES [67] that the anomalously strong temperature dependence of ARPES cannot be explained in terms of the simple polaron effect. It was also shown [186] that the pure $t-J$ model cannot explain effects observed in experiment. Hence, the temperature

dependence of ARPES in the framework of $t-J$-H models was studied in Ref. [56], where the EPC, which appeared to be useful in the interpretation of other properties, was taken into account. Comparison of theoretical and experimental results, showing the importance of contributions to the temperature dependence of both lattice and magnetic degrees of freedom, is considered in Section 4.5.

One more proof of the importance of the interplay between the magnetic and lattice degrees of freedom can be obtained from an analysis of the structure of optical absorption spectra of weakly doped compounds. A two-peak structure in the infrared range, which was vaguely seen in experimental spectra long ago (see Fig. 3 in Ref. [35], Fig. 9 in Ref. [31], and Refs [187–192]), was clearly revealed in recent experiments [57]. Section 4.6 contains the results of calculations of optical absorption spectra of the $t-J$-H model, which explain the two-peak structure of absorption in terms of the joint influence of the magnetic and lattice degrees of freedom. It follows from the analysis of the doping dependence of the optical absorption that a large effective electron–phonon coupling constant $\lambda \sim 1$ decreases with doping, reaching moderate but still considerable strengths ($\lambda \sim 0.5$) at the optimal doping.

The pattern of manifestations of EPC in spectroscopy would not be comprehensive if intensive experimental research of kinks in ARPES were not mentioned. There is no conclusive agreement on the issue of whether kinks are caused by the magnetic resonance mode or by phonons. However, the phonon origin of these famous anomalies can confidently be expected based on recent experiments of the isotope effect in ARPES and kink studies in the ARPES of electron-doped HTSC compounds. A review of these results is given in Section 4.7.

4.1 Influence of the electron–phonon coupling on phonons

EPC leads to a decrease in the phonon energy, and their softening and decay, i.e., to a broadening of the line observed in neutron scattering experiments. Phonon softening was demonstrated by exact diagonalization of the reduced three-band Hamiltonian in a small cluster in one of the earliest theoretical studies [193].

Softening of breathing [with the wave vector $\mathbf{q} = (\pi, \pi)$] and half-breathing [$\mathbf{q} = (\pi, 0)$] phonons was calculated in Refs [102, 103, 106, 111]. Theoretical calculations predicted a doping dependence of softening of those phonons, which was later confirmed in experiment [80]. The results of calculations of phonon broadening [103] showed, in complete agreement with experiment, that the linewidth is maximal at $\mathbf{q} = (\pi, 0)$ and much smaller at $\mathbf{q} = (\pi, \pi)$.

The nature of EPC and its dependence on wave vectors was considered in Ref. [107]. In particular, it was shown that vertex corrections enhance the effective d-symmetry interaction for superconducting pairing of holes at the same wave vectors at which maximal softening and broadening of longitudinal optical phonons is observed in neutron scattering experiments.

The charge response of HTSC compounds due to their ionic nature was considered in Refs [194, 195]. Strong softening of phonons polarized along the c-axis was predicted in these papers before experiments were done.

Phonon softening in the Holstein–Hubbard model was calculated by the dynamical mean field method in Ref. [181], where the Hubbard repulsion U was shown to decrease the phonon softening induced by EPC in an undoped system. However, in agreement with experimentally observed tendencies, phonon softening is enhanced with an increase in doping.

A modification of the $t-J$ model with the EPC taken into account is formulated in Ref. [68] on the basis of *ab initio* calculations in the framework of the three-band model. The phonon spectral function of the above model is studied by the exact diagonalization method. The phonon dispersion calculated at the doping $\delta = 0.125$ agrees with the corresponding experimental data.

4.2 Ghost quasiparticles in photoemission spectra

The spectral function of the $t-J$-H model was previously investigated by the exact diagonalization method on small clusters [196] and in the noncrossing approximation (NCA), where the crossings of phonon and magnon propagators are neglected [197, 198]. However, the small size of the system in the exact diagonalization method implies a discrete spectrum [196, 199], which considerably hampers studies of the lineshape. As regards the NCA, it is applicable to a description of EPC only in the perturbation theory framework [49]. On the other hand, the NCA is valid for describing the coupling to magnons because the spin $S = 1/2$ cannot be flipped more than once, and hence the interaction of polarons with the magnetic subsystem cannot be strong.

A diagrammatic Monte Carlo expansion in Ref. [49] takes the mutual crossing of phonon propagators into account and, to avoid a sign problem, neglects crossings of magnon lines. The NCA for magnons at $J/t \leqslant 0.4$ works properly, as is shown by comparing results obtained in the NCA and in the exact diagonalization method on small clusters [92, 93, 96, 200, 201]. The conclusions in the above references were confirmed by later investigations of the influence of the NCA on results obtained in the $t-J$-H model framework [202]. Recent ARPES calculations [203] conducted by avoiding the NCA variational method [204, 205] also confirmed that omitting diagrams with crossed magnon propagators [49] is meaningful.

The calculated low-energy part of ARPES in the ground state with $\mathbf{k} = (\pi/2, \pi/2)$ in the weak, intermediate, and strong coupling regimes is presented in Fig. 1a–e. The coupling constant dependence of energies of the resonances (Fig. 1f), the $Z^{\mathbf{k}=(\pi/2,\pi/2)}$ factor of the lowest peak (lower inset in Fig. 1f), and the average number of phonons in a polaron cloud $\langle N \rangle$ (upper inset in Fig. 1f) demonstrate the behavior that is typical for self-trapping phenomena [47, 206].

The momentum dependence of the LF is presented in Fig. 2a–d. The location of the quasiparticle polaron peak with a small spectral weight, denoted by a vertical arrow in Fig. 2a–d, barely depends on momentum. The dispersion of the wide shake-off Franck–Condon peak is reasonably well reproduced by the expression (Fig. 2e)

$$\varepsilon_{\mathbf{k}} = \varepsilon_{\min} + \frac{W_{J/t}}{5}\Big\{(\cos k_x + \cos k_y)^2 + \frac{1}{4}\left[\cos(k_x + k_y) + \cos(k_x - k_y)\right]^2\Big\}, \tag{8}$$

which excellently describes the pure $t-J$ model dispersion in a rather wide range of coupling constants, $0.1 < J/t < 0.9$ [96]. We note that the above property of the wide peak dispersion is a general property of the strong-coupling regime.

That the shake-off Franck–Condon peak reproduces the dispersion of particles not coupled to phonons is a direct consequence of the closeness to the adiabatic regime.

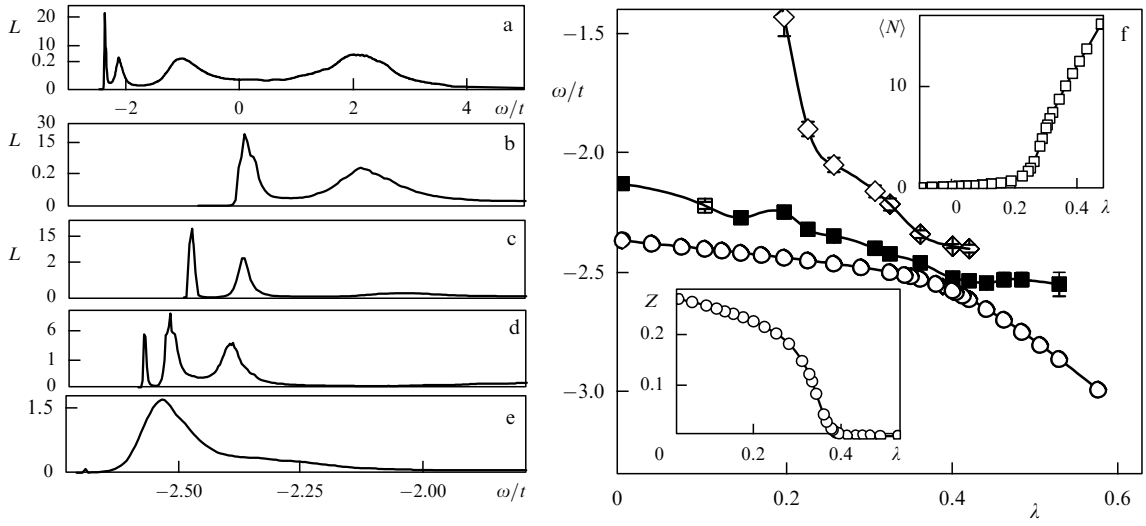

Figure 1. (a) The LF of the ground state with $\mathbf{k} = (\pi/2, \pi/2)$, $J/t = 0.3$, and $\lambda = 0$. The low-energy part of the LF in the ground state with $\mathbf{k} = (\pi/2, \pi/2)$, $J/t = 0.3$ and at $\lambda = 0$ (b), $\lambda = 0.3$ (c), $\lambda = 0.4$ (d), and $\lambda = 0.46$ (e). (e) Dependence of the energies of the lowest resonances, the Z factor of the lowest state (the lower inset), and the average number of phonons $\langle N \rangle$ (the upper inset) on the EPC constant at $J/t = 0.3$.

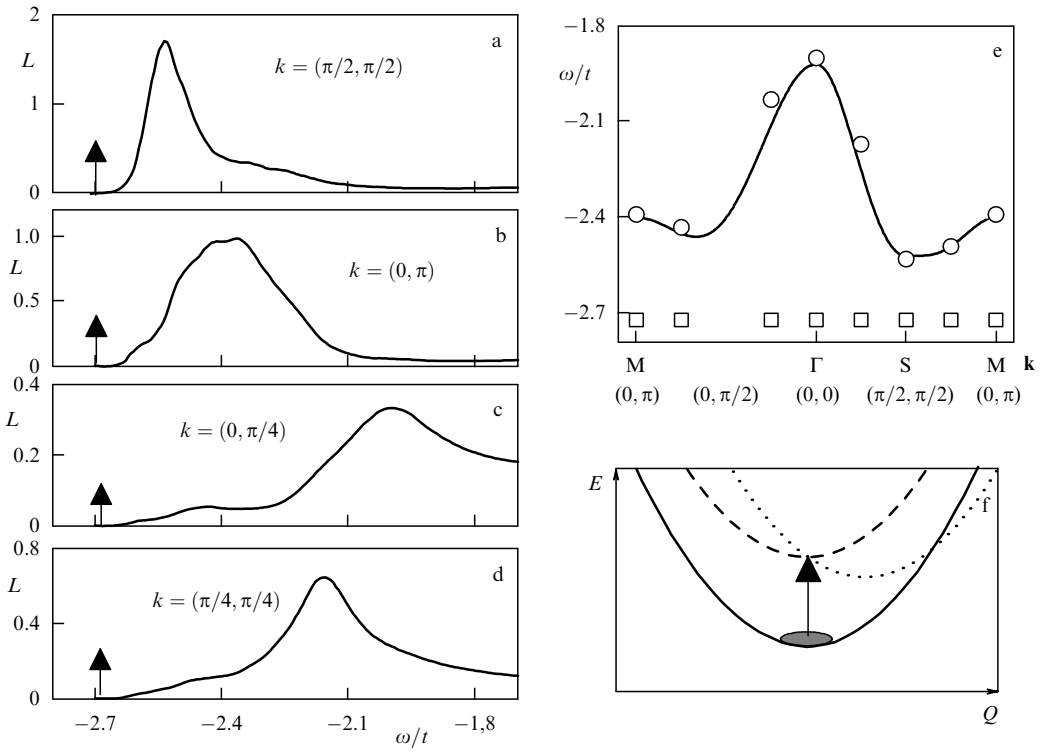

Figure 2. (a–d) Low-energy part of the LF of a hole at $J/t = 0.3$ and $\lambda = 0.46$. Arrows show the location of an invisible low-lying resonance with low weight. (e) Dispersion of energies of resonances at $J/t = 0.3$: a broad resonance (circles) and quasiparticles with low weight (squares) at $\lambda = 0.46$. Solid line is the hole dispersion in the pure $t-J$ model at $J/t = 0.3$ ($W_{J/t=0.3} = 0.6$) and $\varepsilon_{\min} = -2.52$. (f) Ground-state potentials $Q^2/2$ (solid line), the excited-state potential without relaxation $D + Q^2/2$ (dashed line), and the excited-state potential after the relaxation $D + (Q - \lambda)^2/2 - \lambda^2/2$ (dotted line). Photoemission transition of an electron from the ground state, denoted by an ellipse, is shown by the arrow.

Actually, the phonon frequency Ω_0 is much smaller than the bandwidth $2J$ of the $t-J$ model, and the adiabatic parameter $\Omega_0/2J = 1/6 \ll 1$ is small. Moreover, there is one more important parameter in the strong-coupling regime: the ratio of the characteristic experimental measurement time $\tau_{\rm mp} = \hbar/\Delta E$ (where ΔE is the difference between the energy of the ground state of a polaron and that of the shake-off peak) to that of lattice vibration $\tau \approx 1/\Omega_0$. The ratio $\tau_{\rm mp}/\tau$ is much less than unity and, consequently, the fast photoemission process 'sees' ions in a frozen configuration; therefore, the lattice configuration does not change during the electron transition [54, 207]. At low temperatures, the spectral function in the Franck–Condon limit can be represented as a sum of transitions between the lower $E_{\rm low}(Q)$ and upper $E_{\rm up}(Q)$ sheets of the adiabatic potential, which are weighted by the adiabatic wave function of the lower sheet $|\psi_{\rm low}(Q)|^2$

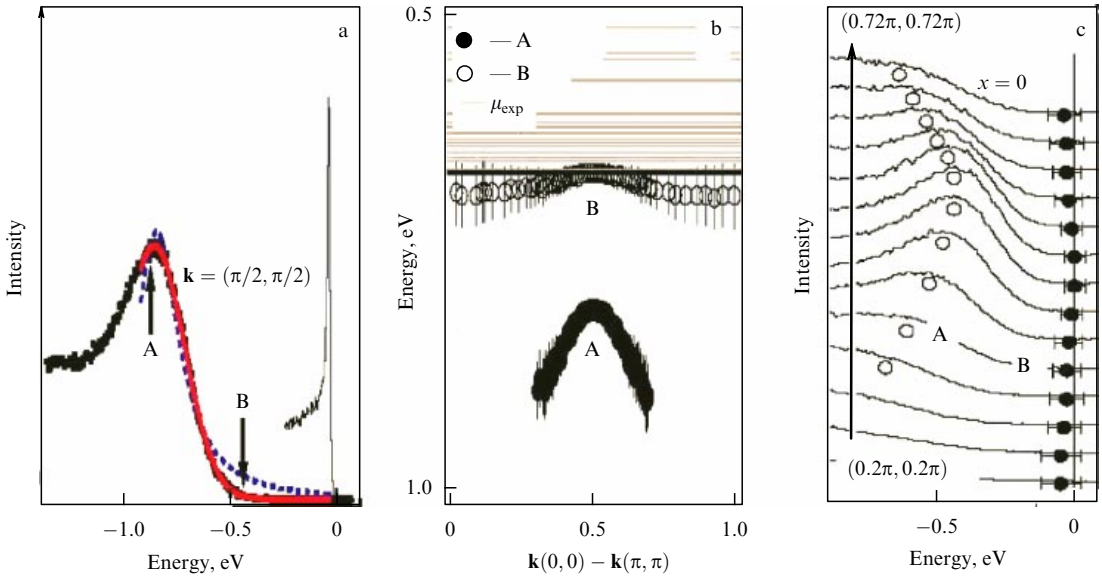

Figure 3. (a) ARPES of undoped $Ca_2CuO_2Cl_2$ at the nodal point $\mathbf{k} = (\pi/2, \pi/2)$ fitted by the Lorentzian (dashed line) and the Gaussian (thick solid line). Points A and B respectively indicate the peak maximum and the energy of the onset of a nonzero spectral density. The narrow peak in the vicinity of zero energy is the ARPES in $SrRuO_4$. (b) Energy dispersion at points A and B. (c) Experimental spectra in the vicinity of the nodal point. (From the data in [66].)

[65]. The spectral peak has a maximum at an energy $\mathcal{D}$ if EPC is absent both in the initial, $E_{\text{low}}(Q) = Q^2/2$, and in the final, $E_{\text{up}}(Q) = \mathcal{D} + Q^2/2$, states of the transition. However, even if the EPC $\Delta E_{\text{up}}(Q) = -\lambda Q$ is present only in the final state, i.e., only when a hole appears in the Mott insulator after the photoemission process, the upper sheet of the adiabatic potential $E_{\text{up}}(Q) = \mathcal{D} - \lambda^2/2 + (Q - \lambda)^2/2$ has the same energy at $Q = 0$. Hence, because the maximum of the probability density $|\psi_{\text{low}}(Q)|^2$ is at $Q = 0$, the peak of the spectral function of the transition broadens but its energy does not shift [65] (Fig. 2f).

The behavior of the peak obtained in calculations corresponds to the behavior of experimental ARPES peaks. The dispersion of the wide peak shown in Fig. 2 reproduces the dispersion of the narrow peak in the t–J model (Fig. 2a–e). The lowest, almost dispersionless, peak corresponding to a small-radius polaron has a small weight, and can therefore be observed only under particular conditions. On the other hand, in agreement with experimental results, the momentum dependence of the broad-peak weight $Z^{(\mathbf{k})'}$ exactly reproduces the behavior of the $Z^{(\mathbf{k})}$ factor of a narrow resonance in the pure t–J model. The reason for this agreement is that in the adiabatic limit $\Omega_0/2J \ll 1$, the whole weight of a sharp resonance transfers to the broad Franck–Condon peak at a strong EPC. The theoretical picture suggested here implies that the chemical potential of weakly doped cuprates is not related to the broad resonances observed in ARPES, but is pinned to a real quasiparticle with a small Z factor. Later, this conclusion was experimentally confirmed in Ref. [66] (Fig. 3). The position of the chemical potential in Fig. 3b is referenced to the energy denoted by point B, and the broad-peak energy at point A is strongly separated from the chemical potential, whose values are shown by the horizontal lines for different samples.

4.3 Estimating the electron–phonon coupling constant λ

The electron–phonon coupling constant λ was most thoroughly determined in Ref. [69]. By that time, the picture suggested in Ref. [49] of an 'invisible' dispersionless particle and a broad shake-off peak had been experimentally confirmed in the ARPES measurement of a $Ca_{2-x}Na_xCuO_2Cl_2$ compound [66]. Hence, the reduced Hamiltonian of the three-band model with a strong EPC [68] was used in Ref. [69] to explain the broad ARPES line of the undoped La_2CuO_4 compound. The knowledge of the EPC strength and structure in the framework of the shell model [113], obtained in Ref. [68], allowed describing anomalies in the phonon dispersion in La_2CuO_4 [68].

The Hamiltonian of the realistic EPC model with 21 phonon modes is given by

$$H_{\text{ep}} = \frac{1}{\sqrt{N}} \sum_{\mathbf{q}\nu i} g_{\mathbf{q}\nu}(1 - n_i)\sqrt{2\omega_{\mathbf{q}\nu}}\, Q_{\mathbf{q}\nu} \exp(\mathrm{i}\mathbf{q}\mathbf{R}_i)\,. \tag{9}$$

Equation (9) describes on-site coupling to holes forming a singlet in the t–J model. The coupling is linear with respect to $Q_{\mathbf{q}\nu}$ and is proportional to the coupling constant $g_{\mathbf{q}\nu}$. The phonon mode of a frequency $\omega_{\mathbf{q}\nu}$ is defined by its wave vector $\mathbf{q}$ and branch index ν, n_i is the electron filling of site $\mathbf{R}_i$, and N is the number of sites.

With the effective coupling constant defined as

$$\lambda \equiv \frac{1}{N} \sum_{\mathbf{q}\nu} \frac{|g_{\mathbf{q}\nu}|^2}{4t\omega_{\mathbf{q}\nu}}\,, \tag{10}$$

the value $\lambda = 1.2$ was obtained in Ref. [69] at $t = 0.4$ eV. The differential spectral distribution of the coupling constant

$$\gamma(\omega) = \frac{1}{N} \sum_{\mathbf{q}\nu} \frac{|g_{\mathbf{q}\nu}|^2}{\omega_{\mathbf{q}\nu}}\, \delta(\omega - \omega_{\mathbf{q}\nu}) \tag{11}$$

was also calculated in Ref. [69]. The authors of Ref. [69] compared spectral distribution (11) with the fine structure of the real part of the quasiparticle spectrum renormalization in the vicinity of the kink measured in Ref. [208]. Good agreement between the above spectral distributions confirms

the phonon nature of the kink, as well as the validity of the estimate of the coupling constant, at least by the order of magnitude.

The scaling $g_{\mathbf{q}\nu} \to \Lambda g_{\mathbf{q}\nu}$ of the coupling constants obtained from reduction of the three-band model was done in Eqn (10) in order to determine the EPC constant from experimental data on the energy difference between the energy of the real quasiparticle and that of the Franck–Condon shake-off peak. The theoretical value of the binding energy (1.2 eV) is considerably larger than the experimental value (0.5 eV) at $\Lambda = 1$. Even a small overestimation of coupling constants caused by an underestimation of screening in the shell model can lead to such an effect, because the binding energy is proportional to Λ^2. A reasonable estimate of the binding energy and the peak width occurs at $\Lambda = 0.8$, which corresponds to the EPC constant $\lambda = 0.75$. Therefore, the approximate value of the EPC constant in cuprates $\lambda \approx 0.75-1.2$ is larger than the critical parameter $\lambda_c = 0.6$ required for the transition of the $t-t'-t''-J$-H model to the strong-coupling regime [52] and for the implementation of the scenario suggested in Ref. [49].

Another source of insight into the EPC strength is the temperature dependence of ARPES in undoped compounds. From a comparison of experimental data in [209] and theoretical estimates for the temperature dependence of the Franck–Condon peak width in [56], it can also be concluded that the EPC constant is in the range $0.5 < \lambda < 1.0$.

The same values were obtained by comparing ARPES and a theoretical calculation of high-energy spectra of the $t-J$-H model. 'Waterfalls' at energies from 1 eV to 2 eV, experimentally observed in ARPES [210–214], were successfully explained as being caused by the behavior of artificially broadened Airy resonances of the $t-J$ model [215, 216]. A subsequent attempt to explain the broadening by a finite temperature and the coupling to phonons showed that taking finite temperature into account is not enough to reproduce the linewidth of high-energy resonances; the EPC must also be involved [217]. The values of parameters $\gamma = 0.5t$ and $\Omega_0 = 0.1t$ [217] give $\lambda = 0.63$ as an estimate of the EPC constant, which is in agreement with other evaluations.

A recent ARPES experiment with electron-doped HTSC compounds $Sm_{2-x}Ce_xCuO_4$ ($x = 0.1,\ 0.15,\ 0.18$), $Nd_{2-x}Ce_xCuO_4$ ($x = 0.15$), and $Eu_{2-x}Ce_xCuO_4$ [218] led to the estimate $\lambda = 0.8$. The coupling constant was determined from a comparison of the abrupt increase in the experimental linewidth occurring as the energy passes through the kink and the theoretical step-like increase in linewidth as it passes through a dispersionless Einstein phonon. The value $\lambda = 0.8$ corresponds well to the results obtained by other methods.

Another method to determine λ was suggested in Ref. [219]. A comparison of the isotope shift of the optical absorption peak in an undoped compound [169] with theoretical results in [220] led to the conclusion that λ is a little larger than unity.

The recently developed electron diffraction technique with time resolution has given the means to study the time evolution of the relaxation of states created under a polarized excitation of carriers [171]. A comparison of experimental results with those obtained in the theory of electron relaxation in metals [221] allows determining λ. The authors of Ref. [171] obtained an anisotropic λ (dependent on crystallographic direction) in the range $0.08 < \lambda < 0.55$.

One more method to estimate the coupling constant λ is associated with the description of high-energy optical absorption by calculations based on the band structure [5, 222–224]. Good agreement with experiment requires large coupling constants $\lambda > 1$ [225, 226]. We also note that a number of calculations by the density functional method [227–231] give values of λ in the range $0.6 \leqslant \lambda \leqslant 1.5$.

4.4 Isotope effect in photoemission

The aim of ARPES studies of the isotope effect (IE) was the kink in quasiparticle dispersion observed in HTSC systems at sufficiently high doping. A report on an extraordinarily strong IE due to the substitution of O^{18} for O^{16} involving a shift of dispersion by more than 10 meV [183, 232] was greeted with much skepticism not mainly because of the large magnitude of the shift but because the isotope shift was observed both close to the energy of the kink and at energies up to several hundred meV.

D Dessau's group invested much effort to verify the results in Refs [183, 232]. Measurements showed that an anomalous IE at high energies is absent and all shifts in ARPES correspond to a change of the phonon frequency by 3 meV induced by isotope substitution [184]. It was noted that even a tiny angle shift of 0.1° in the sample can lead to considerable shifts in high-energy dispersion. The authors of Ref. [184] point out that their result is compatible with the results of tunnel experiments [233, 234], where a 3 meV shift of spectral features was observed. A disagreement with the results in Refs [183, 184, 232] was explained in Ref. [235] by different levels of doping of the samples under study.

The most detailed analysis of the IE in ARPES was done in Ref. [182]. A shift of dispersion is observed only in the vicinity of the kink and its characteristic value is (3.4 ± 0.5) meV. The amazing precision of the data obtained in Ref. [182] results from implementation of a novel low-energy method for ARPES measurements, whose resolution is considerably higher than that of conventional ones [236]. The results of the corresponding IE calculations show that the breathing mode at the energy 70 meV has to shift after the isotope substitution by 3.9 meV, which is in good agreement with the experimentally found value.

The IE has been studied theoretically in many papers. The Holstein model was studied by the path integral method [116] in Refs [237–240] and by the dynamical mean field theory in Ref. [241]. The influence of isotope substitution on mass appeared to be especially strong when the system is close to the crossover to the strong-coupling regime. The IE and its influence on ARPES were studied in Ref. [242] using the susceptibility of the Kampf–Schrieffer model [243]. The IE in the Hubbard–Holstein model was considered in Refs [244–246].

Studies of the IE in ARPES in the framework of the realistic three-band model [247] should be singled out from numerous papers on the IE. The interplay of the EPC and electron correlations is not taken into account in Ref. [247], although the realistic nature of the three-band model allows coming to a number of useful conclusions. The strongest IE is observed in the vicinity of the phonon frequency, the same as in experiment [182]. The authors of Ref. [247], based on a consideration of the contribution of the electron subsystem to the renormalization of ARPES, conclude that the kink cannot be caused by the electron–electron interaction and is caused by the EPC instead.

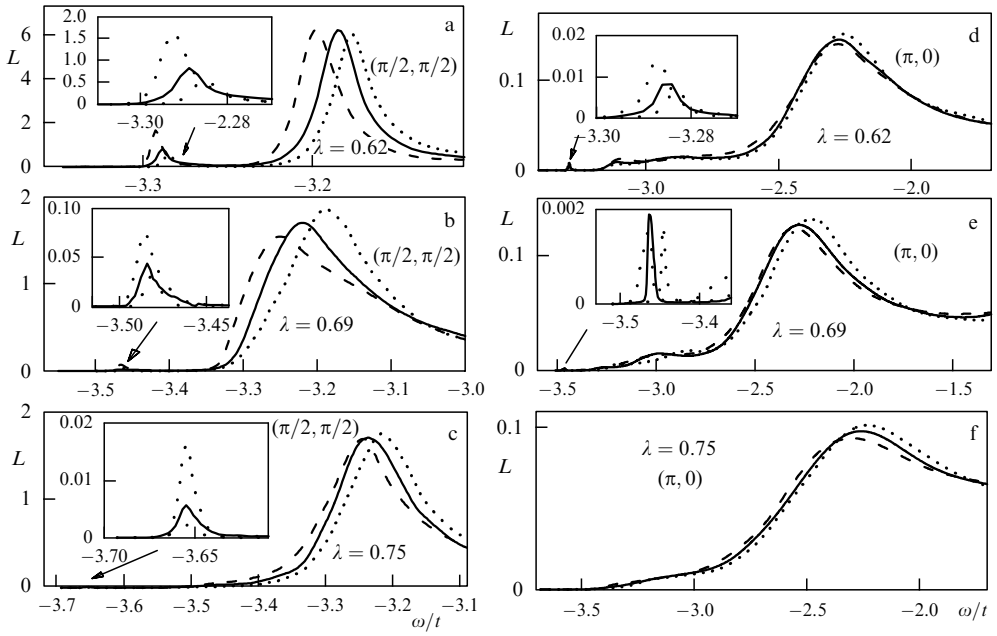

Figure 4. Low-energy part of the LF of a hole: normal compound (solid line), isotope-substituted compound (dotted line), and 'anti-isotope'-substituted compound (dashed line). The LFs at different couplings in the nodal $(\pi/2, \pi/2)$ (a–c) and antinodal $(\pi, 0)$ (d–f) points. A low-energy peak of the real quasiparticle is shown in the insets.

Presently, it is important to perform experiments studying the IE in undoped compounds. Apart from HTSC compounds, there is a variety of other systems where the mechanism of ARPES broadening induced by a strong EPC can be one of the competing scenarios. Diatomic molecules [248], manganites with colossal magnetoresistance [249], quasi-one-dimensional Peierls conductors [250, 251], and Verwey magnetites [252] belong to such systems.

A theoretical study of the IE in undoped compounds was performed in Ref. [52]. The dispersionless coupling constant $\lambda = \gamma^2/4t\Omega$ in Eqn (4) is an invariant in the simplest case of the IE. For the standard relation $\Omega \sim 1/\sqrt{M}$ between the phonon frequency and mass, the dispersionless electron–phonon coupling constant λ is independent of the isotope factor $\kappa_{\rm iso} = \Omega/\Omega_0 = \sqrt{M_0/M}$, which is defined as the ratio of phonon frequencies of isotope-substituted (Ω) and normal (Ω_0) systems. The parameters t, t', t'', and J are chosen to reproduce well the ARPES dispersion in undoped systems [13]: $J/t = 0.4$, $t'/t = -0.34$, and $t''/t = 0.23$. The phonon frequency is chosen as $\Omega_0 = 0.2t$ and the isotope factor for the substitution of O^{18} for O_{16} is set to $\kappa_{\rm iso} = \sqrt{16/18}$ [12].

To guarantee the stability of the analytic continuation of DMC results in imaginary time to real frequencies, LFs were calculated in Ref. [52] for normal $(\kappa_{\rm nor} = 1)$, isotope substituted $(\kappa_{\rm iso} = \sqrt{16/18})$, and 'anti-isotope'-substituted $(\kappa_{\rm ant} = \sqrt{18/16})$ compounds. The monotonic dependence of the LF on κ proves the stability of the spectral analysis and allows evaluating error bars for any calculated quantity $\mathcal{A}$ using the results for $\mathcal{A}_{\rm iso} - \mathcal{A}_{\rm nor}$, $\mathcal{A}_{\rm nor} - \mathcal{A}_{\rm ant}$, and $(\mathcal{A}_{\rm iso} - \mathcal{A}_{\rm ant})/2$.

Figure 4 shows the IE in the low-energy part of the LF of a hole at the nodal and antinodal points at different values of the EPC constant. The shift of all spectral signals to higher energies as the isotope mass increases is obvious $(\kappa < 1)$. We note that the shift of the broad Franck–Condon peak (FCP) is larger than that of the narrow peak of a real quasiparticle. Moreover, the shift of the energy of a quasiparticle tends to zero at large λ and the IE results in a decrease in the spectral weight Z as the isotope mass increases. On the other hand, the shift of the FCP is not suppressed at a strong EPC. There is the following characteristic feature of the IE occurring in all the considered cases except the one where the LF is in the nodal point at $\lambda = 0.62$ (Fig. 4a) and the weight of the quasiparticle described by the δ-function is still large. The FCP height increases as the isotope mass increases. Using the sum rule $\int_{-\infty}^{+\infty} L_{\mathbf{k}}(\omega)\,{\rm d}\omega = 1$ for the LF and nonsensitivity of the high-energy part of the LF to the EPC strength [52], we can conclude that the FCP becomes narrower as the isotope mass increases. To clarify the main tendencies of the IE in the strong-coupling regime, the exactly solvable independent oscillator model (IOM) [253] was analyzed in Ref. [52]. The LF of the IOM is given by the Poisson distribution

$$L(\omega) = \exp\left(-\frac{\xi_0}{\kappa}\right) \sum_{l=0}^{\infty} \frac{[\xi_0/\kappa]^l}{l!}\, \mathcal{G}_{\kappa,l}(\omega)\,, \qquad (12)$$

where $\xi_0 = \gamma_0^2/\Omega_0^2 = 4t\lambda/\Omega_0$ is a dimensionless coupling constant for the initial system and $\mathcal{G}_{\kappa,l}(\omega) = \delta(\omega + 4t\lambda - \Omega_0\kappa l)$ is the delta function. The properties of the Poisson distribution explain many properties of the IE in the LF.

The energy $\omega_{\rm QP} = -4t\lambda$ of the zeroth phonon line $l = 0$ in expression (12) is independent of the isotope factor. This explains the weak isotope dependence of the quasiparticle energy, which is seen in the insets of Fig. 4. In the IOM, in addition, the change in the weight $Z^{(0)}$ of the zeroth phonon line is expressed by the relation

$$\frac{Z_{\rm iso}^{(0)}}{Z_{\rm nor}^{(0)}} = \exp\left[-\frac{\xi_0(1-\kappa)}{\kappa}\right].$$

Estimates in the IOM framework coincide with DMC data within 15% at the nodal and 25% at the antinodal point. The

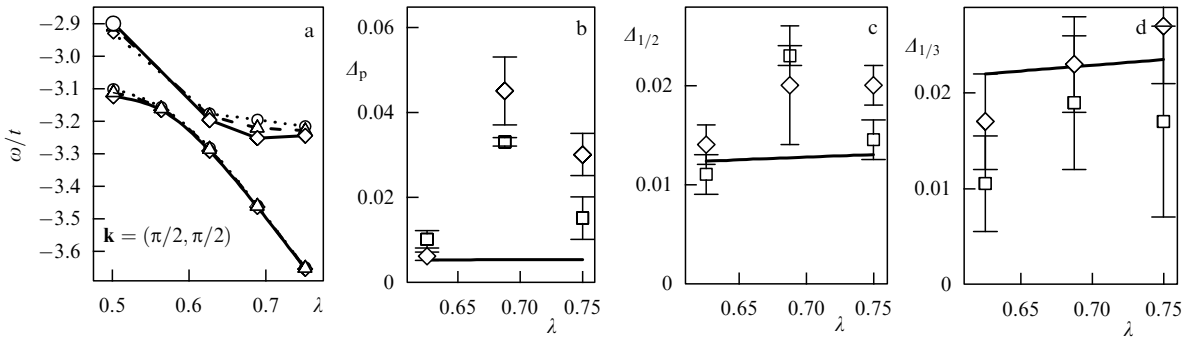

Figure 5. (a) Energies of the ground state and broad peaks in normal (triangles), isotope-substituted (circles), and 'anti-isotope'-substituted (rhombi) compounds. Comparison of estimated IE in IOM (lines) with data of the exact calculation at the nodal (squares) and antinodal (rhombs) points: (b) shift of the top of the FCP, (c) shift of the leading edge of the FCP at half width, and (d) shift of the leading edge of the FCP at one third of the height.

IE at the FCP in the strong-coupling regime follows from the properties of the zeroth $M_0 = \int_{-\infty}^{+\infty} L(\omega)\,\mathrm{d}\omega = 1$, first $M_1 = \int_{-\infty}^{+\infty} \omega L(\omega)\,\mathrm{d}\omega = 0$, and second $M_2 = \int_{-\infty}^{+\infty} \omega^2 L(\omega)\,\mathrm{d}\omega = \kappa\xi_0\Omega_0^2$ moments of shifted Poisson distribution (12). The moments M_0 and M_2 predict the ratio $\mathcal{D} = h_{\mathrm{iso}}^{\mathrm{FCP}}/h_{\mathrm{nor}}^{\mathrm{FCP}} = 1/\sqrt{\kappa} \approx 1.03$ of the FCP heights for normal and isotope-substituted compounds. The above estimate is in perfect agreement with the DMC data at the antinodal point at any of the considered values of the EPC constant. Agreement at the nodal point is observed only at $\lambda = 0.75$ ($\mathcal{D} \approx 1.025$); at smaller λ, the system is not yet described by the strong-coupling regime at this wave vector. A shift of the low-energy FCP edge by the half-height $\Delta_{1/2}$ has to be proportional to the change of the square root of the second moment $\Delta_{\sqrt{M_2}} = \sqrt{\xi_0}\,\Omega_0[1 - \sqrt{\kappa}]$. As was shown in numeric simulations with Gaussians $\mathcal{G}_{\kappa,l}(\omega)$ instead of δ-functions, the relation $\Delta_{1/2} \approx \Delta_{\sqrt{M_2}}/2$ holds within 10% in the range $0.62 < \lambda < 0.75$. It is also established that the shift of the low-energy edge at one third of the height $\Delta_{1/3}$ obeys the relation $\Delta_{1/3} \approx \Delta_{\sqrt{M_2}}$. The results of the DMC method agree well with those obtained in the IOM at a strong EPC, $\lambda = 0.75$ (Fig. 5). However, both FCP shifts, Δ_{p} and $\Delta_{1/2}$, are considerably enhanced in the self-trapping region. The physical reason for the enhancement in this region is common to all regimes and conditions. The effect of the nonadiabatic matrix element, mixing of the ground and excited states, considerably depends on the phonon frequency. The transition is abrupt and nonanalytic in the adiabatic approximation [206], whereas the nonadiabatic matrix element turns the transition into a smooth crossover [254]. Hence, the smaller the frequency, the sharper the bend in the dependence of energies of excited states on λ.

Theoretical results for undoped compounds [52] do not involve any approximations except the NCA for magnons, which is quite applicable in this domain of parameters [202]. The IE in ARPES is considerably enhanced in the range of parameters putting the system into the vicinity of self-trapping crossover, whereas the IE in the strong-coupling regime can be described well by the independent oscillator model. The shift of the FCP top is an easily measured quantity in the intermediate-coupling regime, because the shift is considerably enhanced in this regime. On the other hand, the shift of the leading edge of the FCP is convenient for measuring quantities in the strong-coupling regime because this shift increases with an increase in the EPC as $\sqrt{\lambda}$.

4.5 Anomalous temperature dependence of photoemission spectra

The unique feature of weakly doped HTSC compounds is a firm link between the EPC and the coupling to the magnetic subsystem. The striking consequence of this link is the unique temperature dependence of ARPES. Actually, the experimental temperature dependence scale is much larger than that predicted by the conventional polaron theory [67]. The magnetic subsystem itself is not a proper candidate for the factor responsible for the anomalous temperature dependence [186] because the typical magnon energy scale $2J \approx 0.2$ eV is even larger than the typical phonon energy $\Omega_0 \approx 0.04$ eV. Recent studies have revealed one more puzzling fact questioning the polaronic scenario. The temperature dependence of the FCP linewidth is linear in the range 200 K $< T <$ 400 K [209] and vanishes when extrapolated to $T = 0$.

Until recently, the ARPES properties in the t–J-H model (limited only to zero temperature) were studied by the exact diagonalization method [196, 255, 256], the NCA [197, 198], and the DMC method [49, 52]. The main difficulty in studying the t–J-H model in (2)–(4) is the presence of completely different couplings of a hole to bosons. The ARPES of the t–J-H model for nonzero temperatures were studied in Refs [56, 257], where the temperature dependence of ARPES was considered using the hybrid dynamical momentum average method (HDMAM). HDMAM is a self-consistent method that combines the advantage of preserving information about the magnon dispersion momentum average method (MAM) [258–266] and that of the dynamical mean field method (DMFM) [267–277], which, in turn, can successfully take strong but local interaction with the lattice into account.

The couplings of a hole to phonons and magnons are significantly different in spite of similar energy scales characterizing the phonon and magnon subsystems. The coupling to magnons is always weak and strongly depends on momentum, whereas the coupling to phonons is strong but local. Actually, the inability of spin $S = 1/2$ to flip more than once restricts the number of magnons to one per site [278]. Therefore, the NCA is a reasonable approximation, at least for small values of J/t [93, 202]. On the other hand, the NCA fails to describe the EPC already in the intermediate-coupling regime [49]. Hence, as concerns the t–J-H model, it is enough to consider magnons depending on momentum in the NCA framework, while summing the lattice degrees of freedom by a nonperturbative method. The MAM and

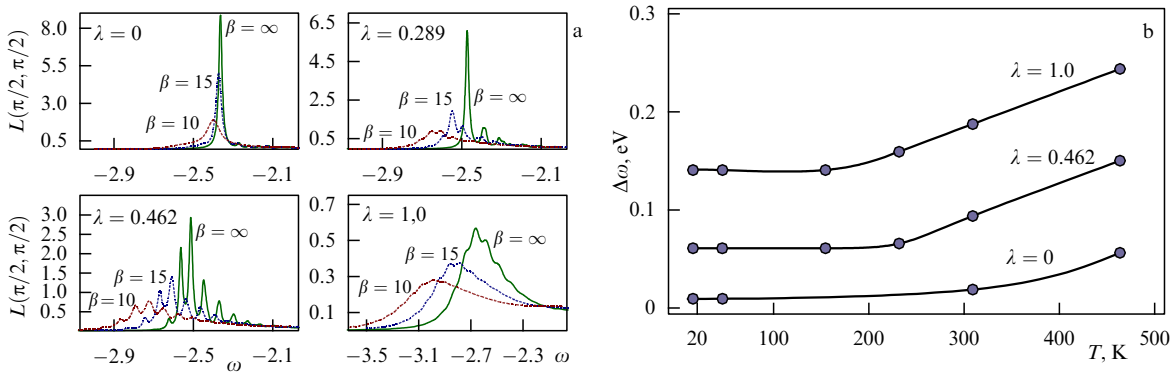

Figure 6. (a) The LF at different values of the EPC constant λ and temperature $\beta = t/T$. (b) The width $\Delta\omega$ as a function of temperature T for the t–J model ($\lambda = 0$) and the t–J-H model in the limit of strong EPC ($\lambda = 0.462$ and $\lambda = 1$). The temperature T (in Kelvin units) is determined under the assumption that $t = 0.4$ eV.

DMFM are nonperturbative methods (valid for any coupling strength) that neglect the momentum dependence of self-energy. The self-energy of a hole due to the EPC can be expressed as a continuous fraction in the framework of the above methods:

$$\Sigma_{\text{h-ph}}\bigl[\alpha(\omega)\bigr] = \cfrac{\gamma^2\alpha(\omega-\Omega_0)}{1-\cfrac{2\gamma^2\alpha(\omega-\Omega_0)\,\alpha(\omega-2\Omega_0)}{1-\cfrac{3\gamma^2\alpha(\omega-2\Omega_0)\,\alpha(\omega-3\Omega_0)}{1-\ldots}}}\,. \tag{13}$$

The difference between the MAM and DMFM is in the definition of the function $\alpha(\omega)$, which is obtained in a self-consistent procedure in the DMFM but is related to the bare Green's function averaged over momenta $\mathbf{k}$ in the MAM. Hence, the total self-energy in the procedure suggested in Ref. [56] is given by the sum of contributions coming from magnetic and lattice subsystems:

$$\Sigma_{t\text{-}J\text{-H}}(\mathbf{k},\omega) = \Sigma^{\text{SCBA}}_{\text{h-mag}}(\mathbf{k},\omega) + \Sigma_{\text{h-ph}}\bigl[\alpha_{t\text{-}J\text{-H}}(\omega)\bigr]\,. \tag{14}$$

The weak anisotropic coupling to magnons is taken into account in the NCA framework:

$$\Sigma^{\text{SCBA}}_{\text{h-mag}}(\mathbf{k},\omega) = \sum_{\mathbf{q}} \frac{M^2_{\mathbf{k},\mathbf{q}}}{\omega-\omega_{\mathbf{q}}-\Sigma_{t\text{-}J\text{-H}}(\mathbf{k}-\mathbf{q},\,\omega-\omega_{\mathbf{q}})+\mathrm{i}\varepsilon}\,, \tag{15}$$

and the function $\alpha(\omega)$ for the phonon self-energy of a hole,

$$\alpha_{t\text{-}J\text{-H}}(\omega) = \frac{1}{N}\sum_{\mathbf{k}} \frac{1}{\omega-\Sigma^{\text{SCBA}}_{\text{h-mag}}(\mathbf{k},\omega)+\mathrm{i}\varepsilon}\,, \tag{16}$$

is expressed in terms of a momentum-averaged Green's function, whose dependence on the momentum $\mathbf{k}$ is defined, in turn, by magnon self-energy (15), which is obtained in the NCA framework. The use of the MAM instead of the DMFM in Eqn (16) is decisive because the DMFM cannot even distinguish the t–J model from the t–J_z model, leading to incoherent movement of the hole. In contrast, a comparison with results obtained by the DMA method [49] shows that solutions of Eqns (13)–(16) reproduce not only the ground-state parameters (energy and spectral weight) but also the LF of the hole [56].

An important advantage of the approach in Ref. [56] is that it can be easily generalized to the case of finite temperatures. Using the Matsubara formalism [253, 279] in description of the self-energy $\Sigma^{\text{SCBA}}_{\text{h-mag}}(\mathbf{k},\omega)$ yields

$$\Sigma^{\text{SCBA}}_{\text{h-mag}}(\mathbf{k},\omega) = \sum_{\mathbf{q}} \frac{M^2_{\mathbf{k},\mathbf{q}}\bigl(1+n_{\text{B}}(\omega_{\mathbf{q}})\bigr)}{\omega-\omega_{\mathbf{q}}-\Sigma_{t\text{-}J\text{-H}}(\mathbf{k}-\mathbf{q},\omega-\omega_{\mathbf{q}})+\mathrm{i}\varepsilon} + \sum_{\mathbf{q}} \frac{M^2_{\mathbf{k}+\mathbf{q},\mathbf{q}}\bigl(n_{\text{B}}(\omega_{\mathbf{q}})\bigr)}{\omega+\omega_{\mathbf{q}}-\Sigma_{t\text{-}J\text{-H}}(\mathbf{k}+\mathbf{q},\omega+\omega_{\mathbf{q}})+\mathrm{i}\varepsilon}\,, \tag{17}$$

where $n_{\text{B}}(\omega)$ is the Bose–Einstein distribution. A generalization of Eqn (13) to finite temperatures, suggested in Ref. [56], uses the fact that the $\alpha(\omega)$ function is reduced to a local value independent of the momentum, and hence [270, 271]

$$\Sigma_{\text{h-ph}}\bigl[\alpha(\omega)\bigr] = \alpha^{-1}(\omega) - \sum_{n=0}^{\infty} \frac{(1-x)x^n}{\alpha^{-1}(\omega)-A_n(\omega)-B_n(\omega)}\,, \tag{18}$$

where $x = \exp(-\beta\Omega_0)$,

$$A_n(\omega) = \cfrac{n(g\Omega_0)^2\,\alpha(\omega+\Omega_0)}{1-\cfrac{(n-1)(g\Omega_0)^2\,\alpha(\omega+\Omega_0)\,\alpha(\omega+2\Omega_0)}{1-\cfrac{(n-2)(g\Omega_0)^2\,\alpha(\omega+2\Omega_0)\,\alpha(\omega+3\Omega_0)}{1-\ldots}}}\,,$$

$$B_n(\omega) = \cfrac{(n+1)(g\Omega_0)^2\,\alpha(\omega-\Omega_0)}{1-\cfrac{(n+2)(g\Omega_0)^2\,\alpha(\omega-\Omega_0)\,\alpha(\omega-2\Omega_0)}{1-\cfrac{(n+3)(g\Omega_0)^2\,\alpha(\omega-2\Omega_0)\,\alpha(\omega-3\Omega_0)}{1-\ldots}}}\,.$$

Equations (14) and (16)–(18) are a self-consistent system. The spectral density [258, 265] obtained from this self-consistent system of equations obeys the first three sum rules for any coupling strength and temperature. Hence, the results for the position and width of the peak obtained in the framework of the above method are reliable [56].

The temperature dependence of the LF with $\mathbf{k} = (\pi/2, \pi/2)$ is shown in Fig. 6 for different values of the EPC strength. Tendencies in variations of the position and width of the peak are in agreement with those observed in experiment [67, 180, 209, 280]. The peak width and distance between the FCP energy and the chemical potential increase as the temperature increases. All temperature effects are enhanced when the EPC is present, confirming in this way that just the

interplay of magnetic and lattice fluctuations is responsible for the anomalous behavior of ARPES. The temperature dependence of the peak width is shown in Fig. 6. We note that the peak width is constant at temperatures less than $T \simeq \Omega_0/2 \approx 200$ K if there is a strong coupling to phonons; as the temperature increases in the range $T > 200$ K, the width demonstrates a linear dependence, which, being naively extrapolated to low temperatures, leads to zero width at $T = 0$. Actually, in accordance with experimental data, the width saturates at $T \geqslant \Omega_0/2$ [67, 281]. We also emphasize that the derivative of the linewidth with respect to temperature is independent of the EPC strength at $T \geqslant \Omega_0/2$, whereas the constant component of the Franck–Condon linewidth is a direct consequence of the strong coupling to phonons.

The temperature dependence of high-energy ARPES bands was studied in Ref. [217]. So-called waterfalls, found in ARPES at energies around 1–2 eV, where dispersion in the energy and momentum coordinates becomes parallel to the energy axis [210–214], were successfully described by the $t-J$ model at zero temperature when artificial broadening was added [215, 216]. We note that the Franck–Condon shake-off peaks whose ARPES and optical absorption spectra were studied in Refs [49, 56] have a characteristic energy not more than 0.3 eV, whereas the waterfalls are observed in the high-energy part of the spectral function. The goal of reproducing the broadening using finite temperatures and the coupling to optical phonons was set in Ref. [217]. The authors of Ref. [217] generalized the self-consistent method for solving the Dyson equation [93, 94, 282] to the case of finite temperatures, and took the coupling to optical phonons into consideration. Calculations showed that the EPC must be taken into account to explain the experimentally observed broadening of spectra at high energies.

Another explanation of waterfalls was suggested in Ref. [283]. The peculiar spectral density at high energies is explained by contributions from localized states. As shown in [283], these local states lead to a quick decrease in the peak intensity along selected directions of the Brillouin zone.

4.6 Traces of the electron–phonon coupling in optical conductivity

The optical conductivity (OC) of weakly doped HTSC compounds has the following characteristic features (see [31, 32, 95]). OC in undoped compounds has a peak at the frequency $\sigma(\omega)$ that corresponds to a charge transfer transition between p-orbitals of oxygen and d-orbitals of copper. At low frequencies, a spectral weight connected with the dynamics of holes appears with doping. In particular, with an increase in doping, the weight of the low-energy part of OC, obeying the Drude law, is proportional to the doping concentration x, and the relaxation rate of the Drude theory $1/\tau$ is proportional to temperature T. On the other hand, the OC $\sigma(\omega)$ at intermediate frequencies is not understood well, especially the mid-infrared (MIR) peak at a doping-dependent frequency $\omega_{\mathrm{MIR}} \approx 0.5$ eV, whose interpretation is far from being unambiguous [33]. It became clear long ago that the pure $t-J$ model is unable to explain the experimentally observed MIR peak. The theoretical frequency of the MIR peak corresponds to the energy $2J \approx 0.28$ eV (for typical parameters $t = 0.4$ eV and $J = 0.35t$), which is almost two times smaller than the experimental value 0.5 eV observed at a low doping level. It became evident that it is necessary to check whether the EPC, vividly manifesting itself in ARPES, can shift the theoretical MIR peak to higher energies.

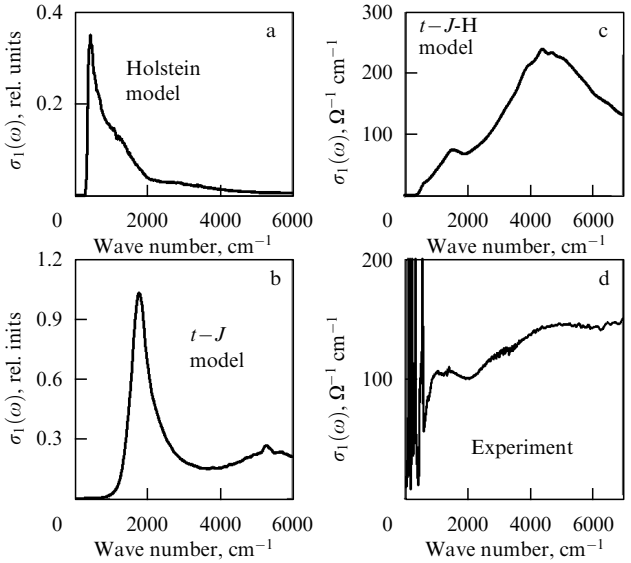

Figure 7. Comparison of the typical OC in different two-dimensional models with experimental data: (a) the Holstein model at $\lambda = 0.44$, (b) the $t-J$ model at $J = 0.3$, (c) the $t-J$-H model at $J = 0.3$ and $\lambda = 0.39$, (d) the in-plain OC of doped (1.5% of holes) $(Eu_{1-x}Ca_x)Ba_2Cu_3O_6$ at $T = 10$ K. The energy scale of theoretical data is given in [cm^{-1}] under the assumption that $t = 0.3$ eV (1 eV = 8065.5 cm^{-1}). The absolute values of the theoretical OC σ_1 were estimated assuming the hopping distance $a = 3.86$ Å and the volume concentration of holes $n_{\mathrm{h}} = 1.72 \times 10^{-23}$ cm^{-3}.

Previously, the OC of the $t-J$-H model was studied by the exact diagonalization method in small clusters [196], in the NCA for phonons and magnons [198], and by the dynamical mean field method in systems of infinite dimension [269]. However, the small size of systems in the exact diagonalization method did not allow studying the fine structure of OC spectra, while the NCA for phonons was not already valid at an intermediate EPC strength. As regards the dynamical mean field method, it is unclear whether the properties of the two-dimensional dynamics of the CuO_2 plain is well reproduced by an infinite-dimensional system.

In Ref. [57], the OC was calculated by the DMC method in a two-dimensional system without the NCA in the phonon channel. The results of calculations were compared with previous experimental data, as well as with new high-resolution measurements performed by the ellipsometry method. The OC is shown in Fig. 7a in the Holstein model (only the EPC), in Fig. 7b in the $t-J$ model (only the coupling to magnons), and in Fig. 7c in the $t-J$-H model. The experimental result is shown in Fig. 7d. There is no agreement with experiment either in the $t-J$ model (Fig. 7b) or in the Holstein model (Fig. 7a). At the same time, the $t-J$-H model reproduces the main features of the experimental spectrum. An explicit feature of the experimental OC, as well as that of the $t-J$-H model, is an apparent two-peak structure: there is a peak at the frequency $\omega_{\mathrm{MIR}} = 4600$ cm^{-1} and a peak at lower energies with the frequency $\omega = 1000$ cm^{-1}, which is located just above the infrared-active phonon modes situated at frequencies below 800 cm^{-1}. The high-energy peak observed in experiment does not correspond to the peak at the frequency $\omega_{t-J} \approx 2J \approx 2000$ cm^{-1} obtained in the pure $t-J$ model (Fig. 7b). The OC of the $t-J$-H model (Fig. 7c) is much closer to the experimental OC (Fig. 7d) because the EPC is taken into account. The peak of the OC in the $t-J$-H model is

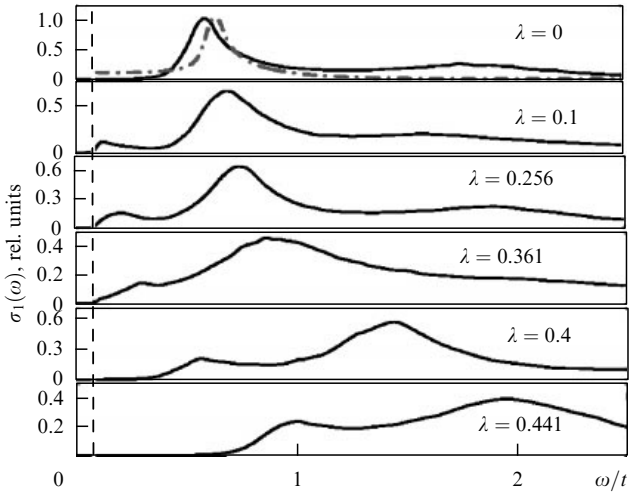

Figure 8. Optical conductivity of one hole in the $t-J$-H model at $J/t = 0.3$ and at different values of the EPC constant λ (solid lines) obtained by the DMC method. Dashed vertical line at $\omega/t = 0.1$ denotes the frequency of phonons. Dash-dotted line in the upper part of the figure is the result obtained from Eqn (19).

considerably shifted to higher frequencies with respect to the peak at the frequency $\omega_{t-J} \approx 2J \approx 2000$ cm^{-1} in the $t-J$ model.

As was shown in Ref. [57], the low-energy OC peak is the phonon sideband with a lower threshold at the phonon frequency [48], while the higher-energy MIR peak is a magnon satellite of the low-energy peak. It is easiest to explain the reason for the shift of the MIR peak to higher energies in the strong-coupling regime, where the Franck–Condon scheme is applicable for OC [54] and energy fluctuations, having the characteristic scale of the Franck–Condon energy, can be considered frozen during the process of optical excitation. In this case, the energy of transition of a hole from the ground state to the excited state of the $t-J$ model with a frozen lattice is the sum of the Franck–Condon energy and the energy of the emitted magnon. Hence, the existence of two peaks and their energies are established by an interplay of the lattice and magnetic subsystems.

All results of calculations of the $t-J$ model OC [17–30] point to the existence of a peak at the frequency $\omega_{t-J} \approx 2J$, whose nature was unknown until recently. It is shown in Ref. [57] that the existence of the peak is connected with the hole transition from the ground state in the coherent $t-J$ band at the wave vector $(\pi/2, \pi/2)$ to another minimum at the point $(-\pi/2, \pi/2)$. The emission of a magnon with the energy $\approx 2J$ and momentum $(\pi, 0)$, accompanying that transition, satisfies the momentum conservation law under the optical transition and defines the peak energy. To prove the leading role of the process described above in the OC of the $t-J$ model, an analytic expression for the OC in the Hilbert space containing only one magnon was considered in Ref. [57] (the result is presented by the dash-dotted curve in Fig. 8):

$$\operatorname{Re}\sigma(\omega) = 4\pi t^2 e^2 (\omega N)^{-1} \sum_{\mathbf{q}} \left| \langle \psi^{(1)}_{\mathbf{k}_0-\mathbf{q}} | O_{\mathbf{q}} | \psi^{(1)}_{\mathbf{k}_0} \rangle \right|^2 \times \delta\left[\omega - \omega_q - \left(E^{(1)}_{\mathbf{k}_0-\mathbf{q}} - E^{(1)}_{\mathbf{k}_0}\right)\right]. \quad (19)$$

Here, $|\psi^{(1)}_{\mathbf{k}}\rangle$ is the lowest basis state with one magnon having the energy $E^{(1)}_{\mathbf{k}}$, $\mathbf{k}_0 = (\pi/2, \pi/2)$, and $O_{\mathbf{q}} = \sum_{\mathbf{k}} h^{\dagger}_{\mathbf{k}-\mathbf{q}} h_{\mathbf{k}} C(\mathbf{k}-\mathbf{q}, \mathbf{k})$. It was found by direct calculation of the sum over $\mathbf{q}$ in (19) that the leading contribution to the OC comes from magnons with momenta in the vicinity of $(\pi, 0)$.

Figure 8 shows the change in OC as the EPC increases. The absorption, in addition to the main MIR peak, shows a peak slightly above the energy of phonons. The two-peak structure of the OC of HTSC compounds can even be seen in data of old measurements (see, e.g., Fig. 3 in [35], Fig. 9 in [31], and [187–192]). But this peak is especially well seen in the low-temperature in-plain OC of weakly doped (1.5% of holes) $Eu_{1-x}Ca_xBa_2Cu_3O_6$, which is measured by the ellipsometry method. This peak, emerging as a consequence of EPC, stays close to phonon energies up to the start of the self-trapping crossover manifesting a transition to the strong-coupling regime, which occurs in the $t-J$-H model at $\lambda \approx 0.4$ [49]. Actually, the dependence of peaks on the coupling constant λ quickly changes at the EPC strength mentioned above (Fig. 9a).

To explain the nature of the low-energy peak, the Holstein model OC with the hopping integral $\tilde{t} = 0.4t$, reduced so as to reproduce the increase in the effective mass in the $t-J$ model, was calculated in Ref. [57]. Self-trapping is observed in this model at $\lambda = 0.4$. As can be seen in Fig. 9b, the effective model described above very well reproduces the low-energy OC peak of the $t-J$-H model.

Considering the dependence of the kink angle in ARPES, it can be supposed that EPC reduces as the doping level increases [70, 285], and the reason for the experimentally observed [33, 34, 36] softening of the MIR peak as the doping increases is the change in the EPC strength. We note that a decrease in the effective EPC for polaron gas is proved theoretically for the Fröhlich model [286–289], although there is no calculation for models with a short-range EPC. A comparison of the experimental position of the MIR peak with the results of the $t-J$-H model gives an estimate [57] for the change in the effective EPC strength as the doping level changes (Fig. 9c, d). Figures 9c and 9d show the ratio of the coupling constant at the current doping level and at zero doping. However, because the absolute value of the EPC coupling constant at zero doping $\lambda(x = 0) \approx 1$ is known from other sources (see Section 4.3), the data in Fig. 9c can be regarded as absolute values of $\lambda^{\mathrm{LSCO}}(x)$. The dependences of the coupling constant on the hole concentration in a plain are very similar in LSCO and YBCO and give quite a universal picture. Figures 9c and 9d give evidence that superconductivity occurs when the effective EPC is already crossing from the strong to the intermediate coupling regime. Although holes are free enough to make their movement coherent, the effective EPC strength $\lambda \approx 0.5$ is still considerable.

Another explanation for the energy dependence of the MIR peak is considered in Refs [269, 290], where the doping dependence of the exchange integral J is suggested instead of the doping dependence of the EPC strength λ proposed in Ref. [57]. Although, regarding only OC, it is difficult to decide between the two debated approaches, the assumption of the doping dependence of λ on concentration easily explains the strong dependence of the kink in dispersion on the hole concentration [70, 119, 208, 291, 285], whereas the approach in [269, 290] does not give a consistent explanation of that dependence. Recently, an experiment in electron-doped compound $Nd_{2-x}Ce_xCuO_4$ was interpreted as an evidence of the independence of λ from concentration [218]. However, it becomes clear from comparison of Fig. 9c and Fig. 4d in Ref. [218] that the range of concentrations considered in

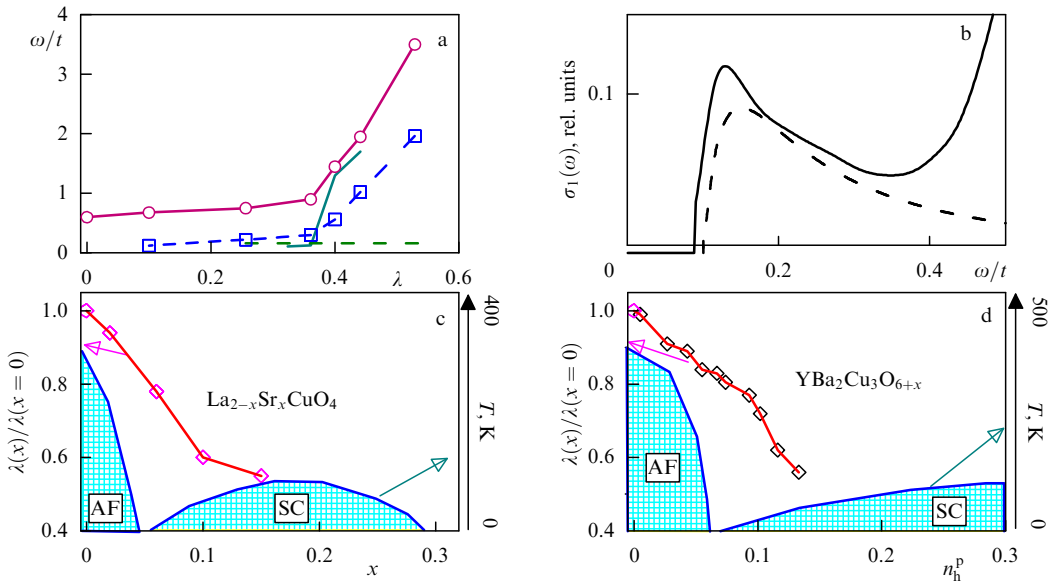

Figure 9. Dependence of energies of the peak dominating in OC (solid line with circles) and of the low-energy peak induced by the EPC (dashed line with squares) on the EPC strength λ. Energy of the dominating peaks in the Holstein model at $t = 1$ (dashed line) and at $\tilde{t} = 0.4$ (solid line). (b) OC of the $t-J$-H model and that of the effective Holstein model with $\tilde{t} = 0.4$ (dashed line) at the same EPC strength $\lambda = 0.1$. Dependence of the ratio $\lambda(x)/\lambda_0$ of the effective electron–phonon coupling constant to its value in an undoped system $\lambda_0 = \lambda(x = 0)$ (c) on the doping concentration x in LSCO and (d) on the 'real' concentration of holes in the copper–oxygen plain in YBCO [284]. The ratio $\lambda(x)/\lambda_0$ was estimated based on the position of the MIR peak. Dependences are superimposed on the corresponding phase diagrams $x-T$ and n_h^p-T; AF is antiferromagnetic state, SC is superconducting state.

measurements is apparently not enough for the confident conclusion that λ is independent of doping.

The OC was also often interpreted in the framework of the polaronic approach in early studies [187, 289, 292–296]. All those papers discussed the structure of OC with one peak and did not consider the complex structure of the spectra observed in experiment. However, another explanation of the two-peak OC structure, not involving the magnetic subsystem in the consideration, appeared recently [297]. The authors of Ref. [297] turn attention to the results of exact calculations of the OC of Fröhlich polarons by the DMC method [48, 54], showing that the two-peak structure is observed at some values of the coupling constant. We note that the two-peak structure is also observed in a certain range of coupling constants in the Holstein model [298]. But the domain of the existence of the two-peak structure is restricted to a narrow range of coupling constants in the Holstein and Fröhlich models, whereas the two-peak structure of OC is a robust property of the $t-J$-H model. An interesting result in Ref. [297], obtained by the method of coherent states [299, 300], is a correlation found between energies of the maxima of OC peaks and ARPES in the strong-coupling limit of EPC. The obtained dependence allows predicting the energy of the OC maximum using that of ARPES, and vice versa. It should be checked in further calculations whether the above correlation is realized in the $t-J$-H model.

A somewhat different interpretation of the low-lying OC peak is given in Ref. [301], where arguments are presented that the peak is associated with local magnetic excitations. In the framework of the interpretation in Ref. [301], the low-lying peak exists in a rather narrow range of parameters. Hence, the above interpretation encounters difficulty in explaining the fact that the peak lying slightly higher than the phonon energies is a robust characteristic feature of numerous HTSC compounds at various doping levels [31, 35, 187–192]. Recently performed calculations [302] show that the peak lying at frequencies slightly above those of phonons is a robust feature of OC. Calculations in [302] were made in the MAM framework, which was improved by the addition of correlated excitations of two and three phonons to basis states.

It is well known that the OC of HTSC compounds is well described at high enough doping levels by the Drude model with a frequency-dependent relaxation time $1/\tau(\omega)$ and the effective mass $m^*(\omega)$ [31, 303]. The frequency dependences of the above quantities, describing experiment, can be obtained in the framework of a strong EPC model [225].

4.7 Kinks in the dispersion of particles

As regards kinks, it is difficult to find another phenomenon in the theory of HTSC compounds that led to such a lengthy confrontation between supporters and opponents of the considerable role played by EPC in those compounds. The typical spectra of different compounds, doping levels, and temperatures are shown in Fig. 10. Initially, the energy 70 meV was attributed to an anomaly [70, 291, 304–309]. However, a more precise analysis in [119, 208] showed that there are lower-energy structures. Kinks are observed not only along the nodal direction $(0, 0)-(\pi, \pi)$ but also in other lines [307–311].

The existence of kinks was explained by the coupling to phonons [109, 110, 247, 312] and to the magnetic resonance mode [310, 313–319] observed in the magnetic neutron scattering of HTSC compounds [320–323]. The authors of Ref. [324] took the interaction with various phonon modes and with the magnetic resonance mode into account, and came to the conclusion that based only on calculations, it is impossible to decide which of the modes causes the kink.

Hence, only experiments can draw the final judgment on the nature of the kink. One of two unambiguous proofs of the phonon nature of the kink was given in [218]. We note

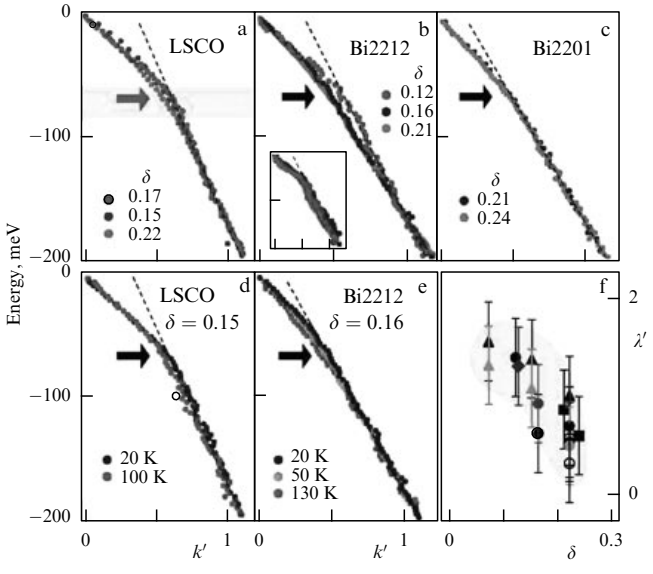

Figure 10. (a–e) Quasiparticle dispersion in the $(0,0)-(\pi,\pi)$ direction in compounds $La_{2-x}Sr_xCuO_4$ (LSCO), $Bi_2Sr_2CuO_6$ (Bi-2201), and $Bi_2Sr_2CaCu_2O_8$ (Bi-2212) at different temperatures and doping levels. (f) The coupling constant λ' determined from changing the dispersion angle using the weak-coupling theory of metal with noninteracting electrons. The quantity $1+\lambda'$ is equal to the ratio of the high speed above the kink energy to the lower speed below the kink energy. The parameter $\lambda' > \lambda$ sets up the upper limit of estimate for the dimensionless EPC constant λ. (Data from [70].)

that the second proof was given in a study of the isotope effect in ARPES [182], published just one month after the appearance of Ref. [218]. As noted in Ref. [218], optical phonons have energies 40 and 70 meV [135, 142] and the magnetic resonance mode is located at the energy 40 meV [320, 325] in hole-doped HTSC compounds. Hence, it is difficult to distinguish between phonon and magnetic scenarios because of the same energy scale of these excitations. However, the phonons of electron-doped HTSC compounds are at the same frequencies, whereas the magnetic resonance mode, as was recently found in Refs [326, 327], is located at 10 meV, which does not corresponds to the energy of the kink. Another proof of the phonon nature of the kink follows from the IE [182]. A shift of dispersion is observed only in the vicinity of the kink and its characteristic value is 3.4 ± 0.5 meV. According to the results of calculations, the breathing mode at 70 meV has to show an isotope shift equal to 3.9 meV, which is consistent with values observed in experiment.

5. Nonlocal nature of the electron–phonon coupling

The simplest model in Eqns (2)–(4) does not explain all the features of HTSC compounds. The reason is that the EPC depends on the wave vector of a phonon, as well on that of a hole [68, 101, 104–109, 111, 112]. Moreover, some properties of the $t-J$-H model are in contradiction with experimental data. For example, the effective mass of the $t-J$-H model is very large in the strong-coupling regime, which is inconsistent with the rather small masses of carriers observed in experiment [33]. An apparent contradiction to experiment was also found in Ref. [256], where it was shown that the strong-coupling regime of the $t-J$-H model leads to a localized static hole with four broken bonds around it. The percolation model predicts that the long-range antiferromagnetic order in this case persists up to the hole concentration $x \approx 0.5$, which is in considerable disagreement with experimental values $x \approx 0.02-0.04$. A similar tendency was noticed in Ref. [328], where it was shown that the EPC helps antiferromagnetism by suppressing the destruction of the antiferromagnetic motion of holes.

Hence, answers to the questions formulated above can be addressed by more realistic $t-t'-t''-J$ models, where the EPC is nonlocal. The study of nonlocal models by the exact diagonalization method [196, 256] is considerably restricted by the small cluster size (usually not more than 10 sites). Based on a coherent states approach [329, 330], a novel method, where coherent-state are treated in the spirit of the Lancos algorithm, was developed in Refs [55, 257]. This method allows obtaining reliable results for the ground state of the $t-t'-t''-J$ model with a nonlocal EPC in two-dimensional systems with 64 sites. The method is verified by comparing its results with those obtained in the $t-J$-H model by the DMC method. As was shown in Ref. [55], local EPC in the $t-t'-t''-J$ model, in contrast to the case of the same local EPC in the $t-J$-H model, produces a different effect on the states of quasiparticles at the nodal $\mathbf{k} = (\pi/2, \pi/2)$ and antinodal $\mathbf{k} = (\pi, 0)$ points. It was also found that the nonlocal EPC considerably changes the main features of the spin–lattice polaron. First, in agreement with general results in [117, 238], the effective mass of the spin–lattice polaron is considerably smaller in the strong-coupling limit than the mass of the polaron with the local EPC. Second, the hopping of holes over nearest neighbors is not suppressed so strongly as it is with the local EPC, and hence the anomalously stable antiferromagnetic order found in the $t-J$-H model does not arise in realistic models.

The minimal Hamiltonian of the $t-t'-t''-J$ model with a nonlocal EPC is the sum of the Hamiltonians of the $t-t'-t''-J$ model, that of phonons with a frequency Ω_0, and the nonlocal EPC operator:

$$H_{\mathrm{h-ph}} = \Omega_0 \sum_l g(l) \sum_{i\in \mathrm{A}} f_i^\dagger f_i (c_{i+l}^\dagger + c_{i+l}) + \Omega_0 \sum_l g(l) \sum_{i\in \mathrm{B}} h_i^\dagger h_i (c_{i+l}^\dagger + c_{i+l}) , \qquad (20)$$

which is defined in terms of the local $g(0) = g$ and nonlocal $g(\boldsymbol{\delta}) = g_1$ coupling constants with displacements of nearest neighbors; f and h are annihilation operators of a hole on two sublattices A and B of the $t-J$ model.

In the framework of the method in [55], the basis states $|h\rangle_j \big[\prod_i |\mu_i\rangle\big] |\mathbf{q}_1, \ldots, \mathbf{q}_l, l\rangle$, where $|h\rangle_j$ is a hole state at site j and i runs over all lattice sites, are defined starting from the hole state in an antiferromagnet. States $|\mathbf{q}_1, \ldots, \mathbf{q}_l, l\rangle$ are restricted to magnons whose lth-order components are enough to reproduce the NCA results [331]. As shown in Ref. [55], the NCA results at $J/t \geqslant 0.3$ can be reproduced by taking only four magnons into account and diagonalizing the resulting truncated basis in the approximation where only the last of the created magnons can be annihilated [332].

The biggest obstacle to solving the problem is considered to be the phonon basis, which previously restricted the size of a system by a cluster of 10 sites [196]. To overcome the difficulty, coherent states (CSs) [329, 330] corresponding to a canonical transformation of the phonon basis were used in

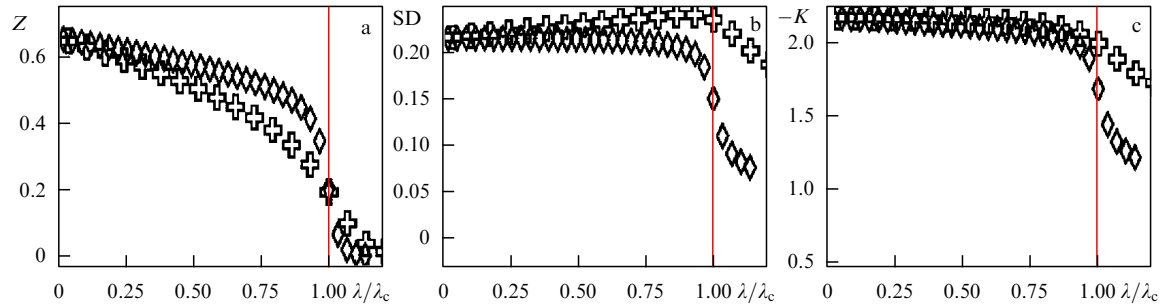

Figure 11. Spectral weight (a), spin deviation around a hole (b), and the average kinetic energy of magnon-induced hops to nearest neighbors (c) at the parameters $J/t = 0.4$, $\Omega_0/t = 0.2$, $t' = -0.5t$, $t'' = 0.4t$, and $N = 16$ for $g_1 = 0$ (rhombi) and $g_1 = 0.5g$ (crosses). The critical λ_c for different models is set at the EPC value at which the spectral weight is reduced by 70% compared with that at $\lambda = 0$.

Ref. [55]:

$$|h, i\rangle = \exp\left[gh(b_i - b_i^{\dagger})\right]|0\rangle_i^{(\mathrm{ph})} = \exp\left(-\frac{g^2h^2}{2}\right)\sum_{n=0}^{\infty}\frac{(-gh)^n}{\sqrt{n!}}\,|n\rangle_i\,. \tag{21}$$

Here, the quantity h is a free parameter. When $h = 0$, the CS is a bare state without the EPC; when $h = 1$, it is the exact solution of the independent-oscillator model with the local coupling g. Comparison of the results obtained in [55] and those given by the DMC method [49] showed that it suffices to restrict the number of states (21) to four in any EPC regime.

To study the influence of the nonlocal EPC on the properties of the system, the $t{-}t'{-}t''{-}J$-H-model was compared with a model involving a coupling to hops to nearest neighbors $g_1 = g/2$ [see (20)]. Figure 11 shows the dependence on the EPC constant of the quasiparticle weight Z in the ground state, spin deviation, and the contribution to the kinetic energy K associated with hops to nearest neighbors. The spin deviation $\mathrm{SD} = (S_{\mathrm{AFM}} - \langle S_{\mathrm{NN}}\rangle)/S_{\mathrm{AFM}}$ is a measure of how much the spin S_{NN} at a site neighboring the hole deviates from the spin S_{AFM} in an ideal antiferromagnet. A decrease in the Z factor is a measure of the suppression of coherent motion of a hole associated with its coherent transfer at a large distance, whereas the absolute value of K and SD are measures of the intensity of hops to nearest neighbors. A decrease in the latter two quantities (Fig. 11b, c) indicates suppression of hole movement to nearest neighbors induced by EPC.

Involvement of a nonlocal EPC leads to the following changes. First, coherent motion is more strongly suppressed at $\lambda < \lambda_c$ and more weakly at $\lambda > \lambda_c$ (Fig. 11a). Second, movement of a hole to nearest neighbors is suppressed considerably more weakly by a nonlocal EPC than by the local Holstein coupling. The above statement can be easily interpreted in the framework of the strong-coupling regime, where the adiabatic potential can be defined. The self-consistent adiabatic potential of a hole is almost δ-functional for the local Holstein coupling, which prevents movement of a hole to nearest neighbors. In contrast, for a long-range EPC with a flat potential well, the hole is not confined to one site, and hence remains mobile even in the strong-coupling regime. Such mobility allows destroying the antiferromagnetic order even in the strong-coupling regime. It is also important that the effective mass of the polaron with a nonlocal EPC is considerably smaller in the strong-coupling regime. For example, for $\lambda = 1.1\lambda_c$, masses differ by an order of magnitude. The diagonal mass (along $k_x = k_y$) is $m_d = 200$ and the perpendicular one (along $k_x = -k_y$) is $m_t = 88$ for the local EPC, whereas $m_d = 20$ and $m_t = 10$ for a nonlocal coupling. A decrease in the strong-coupling effective mass as the EPC range increases has been observed many times in many other models [117, 238, 333–336]. It is interesting to note that a long-range EPC binds two polarons into inter-site bipolarons even if the on-site repulsion is present [337, 338]. These bipolarons can even be superlight in some specific lattice geometries [339].

The nonlocal nature of the coupling must also manifest itself in optical conductivity [14, 340]. For example, the OC peak in the strong-coupling regime of the Holstein model is seen at the energy $2\varepsilon_p$ equal to two binding energies of a polaron, whereas the peak energies are considerably smaller in models with a long-range interaction [340]. This can be explained by the fact that OC is described by a current–current correlation function, while the current operator in lattice models corresponds to electron transitions to a neighboring site. The electron loses an energy ε_p and leaves excited phonons of the same energy at the initial site as it moves to a neighboring site in the Holstein model. Phonons are excited both at the site and far away from the site, which leads to a weaker rearrangement of lattice distortion and, as a consequence, to a decrease in the OC peak energy for a long-range EPC.

Moreover, the fine structure of the coupling is of the same importance as its range. A comparison of the effect of buckling and breathing phonons, distorting the CuO_4 cluster, was made in Ref. [341]. Reduction to the $t{-}J$ model leads to the Hamiltonian

$$H_{\mathrm{Br-Bu}} = \gamma\sum_{i,\boldsymbol{\delta}}(b_{i,\boldsymbol{\delta}} + b_{i,\boldsymbol{\delta}}^{\dagger})(n_i \pm n_{i+\boldsymbol{\delta}})\,, \tag{22}$$

where i is a copper site and the vector $\boldsymbol{\delta} = (x, y)$ denotes different directions of bonds. The plus (minus) sign corresponds to the buckling (breathing) mode. As was shown by the exact diagonalization method [341], the breathing mode suppresses the kinetic energy considerably more strongly than the buckling mode does. The reason is that the breathing phonon decreases the energy at a site, while simultaneously increasing it at a neighboring site. In contrast, the buckling mode decreases and increases the energy on both neighboring sites simultaneously, which prevents effective suppression of kinetic energy. The influence of the EPC structure on polaron properties was studied in detail in Refs [117, 237, 238, 335]. Spectral properties of the Holstein polaron and of a polaron coupled to the breathing mode were compared in Ref. [342].

6. Influence of correlations and other factors on manifestations of the electron–phonon coupling

To analyze the role of EPC properly, it is necessary to indicate precisely which properties of the system are under consideration. For example, the nature of the influence of EPC on electrons and phonons is qualitatively different. Let a hole (phonon) have the dispersion $\varepsilon(\mathbf{k}) = \epsilon(\mathbf{k})$ ($\varepsilon(\mathbf{k}) = \omega(\mathbf{k})$) in a system without the EPC. In a noninteracting system, the spectral function $S(\mathbf{k},\omega)$ observed in ARPES (neutron scattering) experiments is a delta-function $S(\mathbf{k},\omega) = \delta(\omega - \varepsilon(\mathbf{k}))$. The EPC results in the self-energy part of the Green's function of the hole (phonon) $\Theta(\mathbf{k},\omega) = \Sigma(\mathbf{k},\omega)$ ($\Theta(\mathbf{k},\omega) = \Pi(\mathbf{k},\omega)$), which turns the experimentally observed spectral function into

$$S(\mathbf{k},\omega) = \frac{1}{\pi} \frac{\left|\operatorname{Im}\Theta(\mathbf{k},\omega)\right|}{\left[\omega - \varepsilon(\mathbf{k}) - \operatorname{Re}\Theta(\mathbf{k},\omega)\right]^2 + \left[\left|\operatorname{Im}\Theta(\mathbf{k},\omega)\right|\right]^2}. \tag{23}$$

The imaginary part $\left|\operatorname{Im}\Theta(\mathbf{k},\omega)\right|$ determines the EPC-induced broadening.

A sum rule for the phonon self-energy [102, 343],

$$\frac{1}{\pi N}\sum_{\mathbf{k}\neq 0}\int_{-\infty}^{\infty}\left|\operatorname{Im}\Pi(\mathbf{k},\omega)\right|\mathrm{d}\omega \approx \gamma^2\left[2\delta(1-\delta)\right], \tag{24}$$

is satisfied in the t–J model where the Hubbard repulsion $U \to \infty$ and charge fluctuations are completely suppressed. Here, N is the number of sites in the system and δ is the concentration of doped holes, which is equal to zero in a half-filled system. Naturally, there is strictly one electron per site for an infinite Coulomb repulsion U, charge fluctuations are suppressed, and there is no influence on phonons as $\delta \to 0$. Empty states appear and the EPC contribution to the phonon width increases as δ increases. On the other hand, it is not necessary to dope the system for a strong contribution of the EPC to the spectra of electronic quasiparticles. The sum rule

$$\frac{1}{\pi}\int_{-\infty}^{0}\operatorname{Im}\Sigma(\mathbf{k},\omega - \mathrm{i}0^+)\,\mathrm{d}\omega = \gamma^2 \tag{25}$$

can be obtained for the self-energy of a hole at $\delta = 0$ [343]. Hence, the influence of EPC on ARPES is strong even in the half-filled system. The physical reason is that even in the half-filled system, ARPES itself creates a hole, which is a charge whose fluctuations are not suppressed by the Coulomb repulsion. Sum rules for the self-energy of the Holstein–Hubbard model were also studied in Ref. [344].

To summarize the results of studies of the influence of strong correlations (i.e., the Coulomb repulsion U) on EPC, we can say that U suppresses the EPC. Calculations performed in the framework of the dynamical mean field approach [345–347] showed that the influence of EPC is strongly suppressed in a paramagnetic system. The presence of an antiferromagnetic state considerably enhances the role of EPC compared to its role in a paramagnetic system [181], although the Coulomb repulsion weakens the EPC in general. It is also shown that doping leads to an additional suppression of the EPC contribution to the electron properties, whereas the EPC contribution to phonon spectral properties increases. The last fact is a direct consequence of sum rule (24).

However, it can be confidently stated that the EPC is stronger in the t–J model than in the Holstein model in the case of one hole at the bottom of the band. This result was obtained by various methods long ago [196, 348–350] and was verified by the diagrammatic Monte Carlo method recently [49]. Comparing the critical constant of the t–J-H model in (2)–(4), $\lambda^{\mathrm{c}}_{t-J} \approx 0.4$ [49], and that of the Holstein model with the same hopping amplitude t, $\lambda^{\mathrm{c}}_{\mathrm{H}} \approx 1$, we conclude that the interaction of a hole with magnons speeds up the transition to the strong-coupling regime. In the case of one hole at the bottom of the t–J model, the situation can be described as follows. The ratio of the effective electron–phonon coupling constants λ in the t–J model and λ_0 in the Holstein model with the bare mass $m_0 = 1/(2t)$ is determined by a variety of factors [14, 197, 202],

$$\frac{\lambda}{\lambda_0} \approx 4Z_0^2\,\frac{\sqrt{m_{\parallel}m_{\perp}}}{m_0}. \tag{26}$$

The factor of reduction $Z_0 < 1$ in the t–J model appears in expression (26) due to a shift of most of the spectral density to high frequencies. On the other hand, two large effective masses of the t–J model coherent band, $m_{\parallel} > m_0$ and $m_{\perp} > m_0$, enhancing the EPC, are a direct consequence of antiferromagnetic correlations. The factor 4, arising because of a fourfold degeneracy of the ground state on wave vectors $(\pm\pi/2, \pm\pi/2)$, becomes very significant for some parameters. For $J/t = 0.2$, the values are $Z_0^2 = 0.05$ and $\sqrt{m_{\parallel}m_{\perp}} = 10m_0$. Hence, the importance of the EPC is doubled in this case, in particular because of the factor 4. For large J/t, e.g., at $J/t = 2$, the enhancement can be considerable ($\lambda/\lambda_0 \approx 16$). It can be concluded that an increase or decrease in the EPC is determined by the fine details of the model, dimension, and filling of the system by electrons. For example, EPC is suppressed by the Coulomb repulsion in the ground state of a Mott dielectric [351], whereas its role in the formation of excitonic spectra of a one-dimensional system is enhanced due to the Coulomb repulsion [352].

One of the factors significantly influencing the role of EPC in the HTSC physics is the inhomogeneous state of samples observed in scanning tunneling spectroscopy experiments [353–355] and in nuclear quadrupole resonance [356]. As shown in Ref. [357], a moderate and even weak EPC can cause dramatic changes to the properties of an inhomogeneous electron gas. This conclusion is confirmed by other calculations [59, 358, 359] in the framework of the DMC method. The influence of EPC is enhanced near surfaces and interfaces [360].

7. Conclusion

The large number of theoretical and experimental results discussed in the current review point to the essential role of EPC in HTSC compounds. Without diminishing the advances achieved in other papers, we can say that the separation of the chemical potential and the wide peaks observed in ARPES experiments, predicted in Ref. [49] and found experimentally in Ref. [66], is one of the results that changed the point of view regarding the physics of undoped HTSC compounds. Furthermore, the analysis in Ref. [69] has shown by several methods that $\lambda \approx 1$ in undoped HTSC compounds. Other papers providing key information about weakly doped compounds include a virtuosic experiment on the isotope effect in kinks of the electron dispersion [182] and

a study of kinks in electron-doped compounds [218]. The role of phonons in kink physics was convincingly demonstrated in [182], and it was shown in [218] that the energy of the kink and that of the magnetic resonance mode, which was long considered to be responsible for the kink, do not coincide in electron-doped compounds.

The results of numerous theoretical studies convincingly demonstrate the importance of phonons in HTSC compounds. Initial simplified models for ideal systems with a short-range EPC at zero temperature have been greatly improved: generalizations are made to the cases of finite temperature and nonlocal EPC, and the case where translation invariance is broken. Further theoretical studies, pretending to a realistic description of HTSC compounds, should develop theoretical methods capable of handling infinite systems at nonzero temperatures and systems with defects without invoking significant approximations.

The author acknowledges N V Prokof'ev, B V Svistunov, E Burovski, Yu Kagan, A S Alexandrov, O P Sushkov, K A Kikoin, N Nagaosa, G De Filippis, V Cataudella, A Sakamoto, Z-X Shen, T P Devereaux, C Bernhard, J Zaanen, G A Sawatzky, K M Shen, K W Kim, H Fehske, T Egami, J Ranninger, C Castellani, C A Perroni, J T Devreese, T Tohyama, O Gunnarsson, G Sangiovanni, E Cappelluti, C Kim, A Alvermann, and M Berciu for their invaluable help in the discussion and formulation of the results. The support of the RFBR grant 07-02-00067a is also acknowledged.

References

1. Andreson P W *The Theory of Superconductivity in the High-T_c Cuprates* (Princeton, NJ: Princeton Univ. Press, 1997)
2. Anderson P W *Science* **316** 1705 (2007)
3. Alexandrov A S *J. Phys. Condens. Matter* **19** 125216 (2007)
4. Alexandrov A S *Phys. Rev. B* **53** 2863 (1996)
5. Maksimov E G *Usp. Fiz. Nauk* **170** 1033 (2000) [*Phys. Usp.* **43** 965 (2000)]
6. Maksimov E G et al. *Pis'ma Zh. Eksp. Teor. Fiz.* **80** 623 (2004) [*JETP Lett.* **80** 548 (2004)]
7. Moussa J E, Cohen M L *Phys. Rev. B* **74** 094520 (2006)
8. Cohen M L *J. Supercond. Novel Magn.* **19** 283 (2006)
9. Pickett W E *J. Supercond. Novel Magn.* **19** 291 (2006)
10. Maksimov E G, Dolgov O V *Usp. Fiz. Nauk* **177** 983 (2007) [*Phys. Usp.* **50** 933 (2007)]
11. Maksimov E G *Usp. Fiz. Nauk* **178** 175 (2008) [*Phys. Usp.* **51** 167 (2008)]
12. Damascelli A, Hussain Z, Shen Z-X *Rev. Mod. Phys.* **75** 473 (2003)
13. Xiang T, Wheatley J M *Phys. Rev. B* **54** R12653 (1996)
14. Gunnarsson O, Rösch O *J. Phys. Condens. Matter* **20** 043201 (2008)
15. Belinicher V I, Chernyshev A L, Shubin V A *Phys. Rev. B* **53** 335 (1996)
16. Belinicher V I, Chernyshev A L, Shubin V A *Phys. Rev. B* **54** 14914 (1996)
17. Rice T M, Zhang F C *Phys. Rev. B* **39** 815 (1989)
18. Stephan W, Horsch P *Phys. Rev. B* **42** 8736 (1990)
19. Poilblanc D, Dagotto E *Phys. Rev. B* **44** 466 (1991)
20. Poilblanc D *Phys. Rev. B* **44** 9562 (1991)
21. Dagotto E et al. *Phys. Rev. B* **45** 10741 (1992)
22. Igarashi J, Fulde P *Phys. Rev. B* **48** 12713 (1993)
23. Jaklič J, Prelovšek P *Phys. Rev. B* **50** 7129 (1994)
24. Jackeli G, Plakida N M *Phys. Rev. B* **60** 5266 (1999)
25. Moraghebi M, Yunoki S, Moreo A *Phys. Rev. B* **66** 214522 (2002)
26. Tikofsky A M, Laughlin R B, Zou Z *Phys. Rev. Lett.* **69** 3670 (1992)
27. Plakida N M *Z. Phys. B* **103** 383 (1997)
28. Eder R, Wróbel P, Ohta Y *Phys. Rev. B* **54** R11034 (1996)
29. Kyung B, Mukhin S I *Phys. Rev. B* **55** 3886 (1997)
30. Dagotto E *Rev. Mod. Phys.* **66** 763 (1994)
31. Basov D N, Timusk T *Rev. Mod. Phys.* **77** 721 (2005)
32. Kastner M A et al. *Rev. Mod. Phys.* **70** 897 (1998)
33. Lee Y S et al. *Phys. Rev. B* **72** 054529 (2005)
34. Cooper S L et al. *Phys. Rev. B* **47** 8233 (1993)
35. Thomas G A et al. *Phys. Rev. B* **45** 2474 (1992)
36. Uchida S et al. *Phys. Rev. B* **43** 7942 (1991)
37. Azzam R M A, Bashara N M *Ellipsometry and Polarized Light* (Amsterdam: North-Holland, 1996)
38. Fluckiger D U *J. Opt. Soc. Am. A* **15** 2228 (1998)
39. Prokof'ev N V, Svistunov B V, Tupitsyn I S *Zh. Eksp. Teor. Fiz.* **114** 570 (1998) [*JETP* **87** 310 (1998)]
40. Prokof'ev N V, Svistunov B V *Phys. Rev. Lett.* **81** 2514 (1998)
41. Mishchenko A S et al. *Phys. Rev. B* **62** 6317 (2000)
42. Mishchenko A S, Nagaosa N *Phys. Rev. Lett.* **86** 4624 (2001)
43. Mishchenko A S et al. *Int. J. Mod. Phys. B* **15** 3940 (2001)
44. Mishchenko A S, Prokof'ev N V, Svistunov B V *Phys. Rev. B* **64** 033101 (2001)
45. Burovski E A et al. *Phys. Rev. Lett.* **87** 186402 (2001)
46. Mishchenko A S et al. *Nonlinear Opt.* **29** 257 (2002)
47. Mishchenko A S et al. *Phys. Rev. B* **66** 020301 (2002)
48. Mishchenko A S et al. *Phys. Rev. Lett.* **91** 236401 (2003)
49. Mishchenko A S, Nagaosa N *Phys. Rev. Lett.* **93** 036402 (2004)
50. Mishchenko A S *Usp. Fiz. Nauk* **175** 925 (2005) [*Phys. Usp.* **48** 887 (2005)]
51. Mishchenko A S, Nagaosa N *J. Phys. Soc. Jpn.* **75** 011003 (2006)
52. Mishchenko A S, Nagaosa N *Phys. Rev. B* **73** 092502 (2006)
53. Mishchenko A S, Nagaosa N *J. Phys. Chem. Solids* **67** 259 (2006)
54. De Filippis G et al. *Phys. Rev. Lett.* **96** 136405 (2006)
55. De Filippis G et al. *Phys. Rev. Lett.* **99** 146405 (2007)
56. Cataudella V et al. *Phys. Rev. Lett.* **99** 226402 (2007)
57. Mishchenko A S et al. *Phys. Rev. Lett.* **100** 166401 (2008)
58. Burovski E, Fehske H, Mishchenko A S *Phys. Rev. Lett.* **101** 116403 (2008)
59. Mishchenko A S et al. *Phys. Rev. B* **79** 180301(R) (2009)
60. Mishchenko A S, in *Polarons in Bulk Materials and Systems with Reduced Dimensionality*: *Proc. of the Intern. School of Physics* '*Enrico Fermi*' Course CLXI (Eds G Iadonisi, J Ranninger, G De Filippis) (Amsterdam: IOS Press, 2006) p. 177
61. Mishchenko A S, Nagaosa N, in *Polarons in Complex Matter* (Springer Series in Material Science, Ed. A S Alexandrov) (Berlin: Springer, 2007) p. 503
62. Mishchenko A S, in *Computational Many-Particle Physics* (Lecture Notes in Physics, Vol. 739, Eds H Fehske, R Schneider, A Weiße) (Berlin: Springer, 2008) p. 367
63. Vafayi K, Gunnarsson O *Phys. Rev. B* **76** 035115 (2007)
64. Wells B O et al. *Phys. Rev. Lett.* **74** 964 (1995)
65. Rösch O, Gunnarsson O *Eur. Phys. J. B* **43** 11 (2005)
66. Shen K M et al. *Phys. Rev. Lett.* **93** 267002 (2004)
67. Kim C et al. *Phys. Rev. B* **65** 174516 (2002)
68. Rösch O, Gunnarsson O *Phys. Rev. Lett.* **92** 146403 (2004)
69. Rösch O et al. *Phys. Rev. Lett.* **95** 227002 (2005)
70. Lanzara A et al. *Nature* **412** 510 (2001)
71. Izyumov Yu A *Usp. Fiz. Nauk* **167** 465 (1997) [*Phys. Usp.* **40** 445 (1997)]
72. Pickett W E *Rev. Mod. Phys.* **61** 433 (1989)
73. Timusk T, Statt B *Rep. Prog. Phys.* **62** 61 (1999)
74. Tohyama T, Maekawa S *Supercond. Sci. Technol.* **13** R17 (2000)
75. Kulić M L *Phys. Rep.* **338** 1 (2000)
76. Alexandrov A S *Theory of Superconductivity*: *From Weak to Strong Coupling* (Bristol: IOP Publ., 2003)
77. Kivelson S A et al. *Rev. Mod. Phys.* **75** 1201 (2003)
78. Norman M R, Pépin C *Rep. Prog. Phys.* **66** 1547 (2003)
79. Norman M R, Pines D, Kallin C *Adv. Phys.* **54** 715 (2005)
80. Pintschovius L *Phys. Status Solidi B* **242** 30 (2005)
81. Lee P A, Nagaosa N, Wen X-G *Rev. Mod. Phys.* **78** 17 (2006)
82. Egami T, in *Polarons in Bulk Materials and Systems with Reduced Dimensionality*: *Proc. of the Intern. School of Physics* '*Enrico Fermi*' Course CLXI (Eds G Iadonisi, J Ranninger, G De Filippis) (Amsterdam: IOS Press, 2006) p. 101
83. Zhou X J et al., in *Handbook of High-Temperature Superconductivity*: *Theory and Experiment* (Ed. J R Schrieffer) (Berlin: Springer, 2007) p. 87; cond-mat/0604284
84. Yoshida T et al. *J. Phys. Condens. Matter* **19** 125209 (2007)
85. Fink J et al. *Lect. Notes Phys.* **715** 295 (2007)
86. Tohyama T *Phys. Rev. B* **70** 174517 (2004)
87. Tohyama T, Maekawa S *Phys. Rev. B* **64** 212505 (2001)
88. Tohyama T, Maekawa S *Phys. Rev. B* **67** 092509 (2003)
89. Kim C et al. *Phys. Rev. Lett.* **80** 4245 (1998)
90. Emery V J *Phys. Rev. Lett.* **58** 2794 (1987)
91. Zhang F C, Rice T M *Phys. Rev. B* **37** 3759 (1988)

92. Kane C L, Lee P A, Read N *Phys. Rev. B* **39** 6880 (1989)
93. Liu Z, Manousakis E *Phys. Rev. B* **45** 2425 (1992)
94. Liu Z, Manousakis E *Phys. Rev. B* **44** 2414 (1991)
95. Manousakis E *Rev. Mod. Phys.* **63** 1 (1991)
96. Marsiglio F et al. *Phys. Rev. B* **43** 10882 (1991)
97. Kyung B, Ferrell R A *Phys. Rev. B* **54** 10125 (1996)
98. Lee T K, Shih C T *Phys. Rev. B* **55** 5983 (1997)
99. Tohyama T, Maekawa S *Phys. Rev. B* **49** 3596 (1994)
100. Lee T K, Ho C-M, Nagaosa N *Phys. Rev. Lett.* **90** 067001 (2003)
101. Devereaux T P, Virosztek A, Zawadowski A *Phys. Rev. B* **51** 505 (1995)
102. Khaliullin G, Horsch P *Phys. Rev. B* **54** R9600 (1996)
103. Khaliullin G, Horsch P *Physica C* **282 – 287** 1751 (1997)
104. Opel M et al. *Phys. Rev. B* **60** 9836 (1999)
105. Devereaux T P, Virosztek A, Zawadowski A *Phys. Rev. B* **59** 14618 (1999)
106. Horsch P, Khaliullin G, Oudovenko V *Physica C* **341 – 348** 117 (2000)
107. Ishihara S, Nagaosa N *Phys. Rev. B* **69** 144520 (2004)
108. Rösch O, Gunnarsson O *Phys. Rev. B* **70** 224518 (2004)
109. Devereaux T P et al. *Phys. Rev. Lett.* **93** 117004 (2004)
110. Cuk T et al. *Phys. Rev. Lett.* **93** 117003 (2004)
111. Horsch P, Khaliullin G *Physica B* **359 – 361** 620 (2005)
112. Bulut N, Scalapino D J *Phys. Rev. B* **54** 14971 (1996)
113. Chaplot S L et al. *Phys. Rev. B* **52** 7230 (1995)
114. Pintschovius L, Reichardt W, in *Neutron Scattering in Layered Cooper-Oxide Superconductors* (Ed. A Furrer) (Dordrecht: Kluwer Acad., 1998) p. 165
115. Timusk T et al., in *Anharmonic Properties of High-T_c Cuprates* (Eds D Mihailović et al.) (Singapore: World Scientific, 1995) p. 171
116. Kornilovitch P E *Phys. Rev. Lett.* **81** 5382 (1998)
117. Alexandrov A S, Kornilovitch P E *Phys. Rev. Lett.* **82** 807 (1999)
118. Meevasana W et al. *Phys. Rev. B* **74** 174524 (2006)
119. Meevasana W et al. *Phys. Rev. Lett.* **96** 157003 (2006)
120. Hohenberg P, Kohn W *Phys. Rev.* **136** B864 (1964)
121. Kohn W, Sham L J *Phys. Rev.* **140** A1133 (1965)
122. Bohnen K-P, Heid R, Krauss M *Europhys. Lett.* **64** 104 (2003)
123. Pintschovius L, Braden M *Phys. Rev. B* **60** R15039 (1999)
124. Giustino F, Cohen M L, Louie S G *Nature* **452** 975 (2008)
125. Reznik D et al. *Nature* **455** E6 (2008)
126. Reznik D et al. *Nature* **440** 1170 (2006)
127. Reznik D et al. *J. Low Temp. Phys.* **147** 353 (2007)
128. Pintschovius L et al. *Phys. Rev. B* **69** 214506 (2004)
129. Uchiyama H et al. *Phys. Rev. Lett.* **92** 197005 (2004)
130. Pintschovius L, Reznik D, Yamada K *Phys. Rev. B* **74** 174514 (2006)
131. Hanaguri T et al. *Nature* **430** 1001 (2004)
132. Kikoin K A, Mishchenko A S *Zh. Eksp. Teor. Fiz.* **94** (11) 237 (1988) [*Sov. Phys. JETP* **67** 2309 (1988)]
133. Kikoin K A, Mishchenko A S *J. Phys. Condens Matter* **2** 6491 (1990)
134. Mishchenko A S, Kikoin K A *J. Phys. Condens Matter* **3** 5937 (1991)
135. McQueeney R J et al. *Phys. Rev. Lett.* **82** 628 (1999)
136. Pintschovius L et al. *Physica C* **185 – 189** 156 (1991)
137. Pintschovius L, Braden M *J. Low Temp. Phys.* **105** 813 (1996)
138. Reichardt W *J. Low Temp. Phys.* **105** 807 (1996)
139. McQueeney R J et al. *Phys. Rev. Lett.* **87** 077001 (2001)
140. Pintschovius L et al. *Phys. Rev. Lett.* **89** 037001 (2002)
141. Chung J-H et al. *Phys. Rev. B* **67** 014517 (2003)
142. Reznik D et al. *Phys. Rev. Lett.* **75** 2396 (1995)
143. Pyka N et al. *Phys. Rev. Lett.* **70** 1457 (1993)
144. Cooper S L et al. *Phys. Rev. B* **37** 5920 (1988)
145. Thomsen C et al. *Phys. Rev. B* **37** 9860 (1988)
146. Macfarlane R M, Rosen H, Seki H *Solid State Commun.* **63** 831 (1987)
147. Franck J P, in *Physical Properties of High Temperature Superconductors IV* (Ed. D M Ginsberg) (Singapore: World Scientific, 1994) p. 189
148. Franck J P et al. *Phys. Rev. B* **44** 5318 (1991)
149. Batlogg B et al. *Phys. Rev. Lett.* **59** 912 (1987)
150. Zech D et al. *Nature* **371** 681 (1994)
151. Zhao G et al. *Nature* **385** 236 (1997)
152. Zhao G et al. *J. Phys. Condens. Matter* **10** 9055 (1998)
153. Zhao G, Keller H, Conder K *J. Phys. Condens. Matter* **13** R569 (2001)
154. Hofer J et al. *Phys. Rev. Lett.* **84** 4192 (2000)
155. Khasanov R et al. *J. Phys. Condens. Matter* **16** S4439 (2004)
156. Khasanov R et al. *Phys. Rev. Lett.* **92** 057602 (2004)
157. Khasanov R et al. *Phys. Rev. B* **74** 064504 (2006)
158. Khasanov R et al. *Phys. Rev. B* **75** 060505(R) (2007)
159. Tallon J L et al. *Phys. Rev. Lett.* **94** 237002 (2005)
160. Khasanov R et al. *Phys. Rev. Lett.* **101** 077001 (2008)
161. Zhao G, Singh K K, Morris D E *Phys. Rev. B* **50** 4112 (1994)
162. Shengelaya A et al. *Phys. Rev. Lett.* **83** 5142 (1999)
163. Raffa F et al. *Phys. Rev. Lett.* **81** 5912 (1998)
164. Rubio Temprano D et al. *Phys. Rev. Lett.* **84** 1990 (2000)
165. Rubio Temprano D et al. *Eur. Phys. J. B* **19** 5 (2001)
166. Rubio Temprano D et al. *Phys. Rev. B* **66** 184506 (2002)
167. Lorenzana J, Sawatzky G A *Phys. Rev. Lett.* **74** 1867 (1995)
168. Lorenzana J, Sawatzky G A *Phys. Rev. B* **52** 9576 (1995)
169. Grüninger M et al. *Phys. Rev. B* **62** 12422 (2000)
170. Bernhard C et al. *Phys. Rev. B* **69** 052502 (2004)
171. Carbone F et al. *Proc. Natl. Acad. Sci. USA* **105** 20161 (2008)
172. Shim H et al. *Phys. Rev. Lett.* **101** 247004 (2008)
173. Sugai S et al. *Solid State Commun.* **76** 371 (1990)
174. Lampakis D, Liarokapis E, Panagopoulos C *Phys. Rev. B* **73** 174518 (2006)
175. Radović Z, Božović N, Božović I *Phys. Rev. B* **77** 092508 (2008)
176. Kim C et al. *Phys. Rev. Lett.* **77** 4054 (1996)
177. Kim C et al. *Phys. Rev. B* **56** 15589 (1997)
178. Brunner M, Assaad F F, Muramatsu A *Phys. Rev. B* **62** 15480 (2000)
179. Leung P W, Gooding R J *Phys. Rev. B* **52** R15711 (1995)
180. Pothuizen J J M et al. *Phys. Rev. Lett.* **78** 717 (1997)
181. Sangiovanni G et al. *Phys. Rev. Lett.* **97** 046404 (2006)
182. Iwasawa H et al. *Phys. Rev. Lett.* **101** 157005 (2008)
183. Gweon G-H et al. *Nature* **430** 187 (2004)
184. Douglas J F et al. *Nature* **446** E5 (2007)
185. Iwasawa H et al. *Physica C* **463 – 465** 52 (2007)
186. Van den Brink J, Sushkov O P *Phys. Rev. B* **57** 3518 (1998)
187. Lupi S et al. *Phys. Rev. Lett.* **83** 4852 (1999)
188. Lupi S et al. *Phys. Rev. B* **45** 12470 (1992)
189. Lupi S et al. *Phys. Rev. B* **57** 1248 (1998)
190. Quijada M A et al. *Phys. Rev. B* **60** 14917 (1999)
191. Onose Y et al. *Phys. Rev. Lett.* **87** 217001 (2001)
192. Wang N L et al. *Phys. Rev. B* **67** 134526 (2003)
193. von Szczepanski K J, Becker K W *Z. Phys. B* **89** 327 (1992)
194. Falter C, Klenner M *Phys. Rev. B* **50** 9426 (1994)
195. Falter C, Klenner M, Hoffmann G A *Phys. Rev. B* **52** 3702 (1995)
196. Bäuml B, Wellein G, Fehske H *Phys. Rev. B* **58** 3663 (1998)
197. Ramšak A, Horsch P, Fulde P *Phys. Rev. B* **46** 14305 (1992)
198. Kyung B et al. *Phys. Rev. B* **54** 13167 (1996)
199. Röder H, Fehske H, Silver R N *Europhys. Lett.* **28** 257 (1994)
200. Schmitt-Rink S, Varma C M, Ruckenstein A E *Phys. Rev. Lett.* **60** 2793 (1988)
201. Martinez G, Horsch P *Phys. Rev. B* **44** 317 (1991)
202. Gunnarsson O, Rösch O *Phys. Rev. B* **73** 174521 (2006)
203. Bonča J et al. *Phys. Rev. B* **77** 054519 (2008)
204. Bonča J, Trugman S A, Batistić I *Phys. Rev. B* **60** 1633 (1999)
205. Bonča J, Maekawa S, Tohyama T *Phys. Rev. B* **76** 035121 (2007)
206. Rashba E I, in *Modern Problems in Condensed Matter Sciences* Vol. 2 (Eds V M Agranovich, A A Maradudin) (Amsterdam: Notrh-Holland, 1982) p. 543; Ioselevich A S, Rashba E I, in *Modern Problems in Condensed Matter Sciences* Vol. 34 (Amsterdam: Notrh-Holland, 1992) p. 347
207. Mishchenko A S *Pis'ma Zh. Eksp. Teor. Fiz.* **66** 460 (1997) [*JETP Lett.* **66** 487 (1997)]
208. Zhou X J et al. *Phys. Rev. Lett.* **95** 117001 (2005)
209. Shen K M et al. *Phys. Rev. B* **75** 075115 (2007)
210. Ronning F et al. *Phys. Rev. B* **71** 094518 (2005)
211. Graf J et al. *Phys. Rev. Lett.* **98** 067004 (2007)
212. Xie B P et al. *Phys. Rev. Lett.* **98** 147001 (2007)
213. Valla T et al. *Phys. Rev. Lett.* **98** 167003 (2007)
214. Meevasana W et al. *Phys. Rev. B* **75** 174506 (2007)
215. Manousakis E *Phys. Rev. B* **75** 035106 (2007)
216. Manousakis E *Phys. Lett. A* **362** 86 (2007)
217. Kar S, Manousakis E *Phys. Rev. B* **78** 064508 (2008)
218. Park S R et al. *Phys. Rev. Lett.* **101** 117006 (2008)
219. Zhao G *Phys. Rev. B* **75** 104511 (2007)
220. Eremin I, Kamaev O, Eremin M V *Phys. Rev. B* **69** 094517 (2004)
221. Allen P B *Phys. Rev. Lett.* **59** 1460 (1987)
222. Mazin I I et al. *Pis'ma Zh. Eksp. Teor. Fiz.* **47** 94 (1988) [*JETP Lett.* **47** 113 (1988)]
223. Maksimov E G et al. *Phys. Rev. Lett.* **63** 1880 (1989)
224. Rashkeev S N et al. *Zh. Eksp. Teor. Fiz.* **97** 1688 (1990) [*Sov. Phys. JETP* **70** 952 (1990)]
225. Shulga S V, Dolgov O V, Maksimov E G *Physica C* **178** 266 (1991)

226. Maksimov E G et al. *Solid State Commun.* **112** 449 (1999)
227. Jarlborg T *Solid State Commun.* **71** 669 (1989)
228. Cohen R E, Pickett W E, Krakauer H *Phys. Rev. Lett.* **64** 2575 (1990)
229. Zeyher R *Z. Phys. B* **80** 187 (1990)
230. Krakauer H, Pickett W E, Cohen R E *Phys. Rev. B* **47** 1002 (1993)
231. Mazin I I et al., in *Lattice Effects in High-T_c Superconductors* (Eds Y Bar-Yam et al.) (Singapore: World Scientific, 1992) p. 235
232. Gweon G-H et al. *Phys. Rev. Lett.* **97** 227001 (2006)
233. Lee J et al. *Nature* **442** 546 (2006)
234. De Lozanne A *Nature* **442** 522 (2006)
235. Gweon G-H et al., arXiv:0708.1027
236. Koralek J D et al. *Phys. Rev. Lett.* **96** 017005 (2006)
237. Hague J P et al. *Phys. Rev. B* **73** 054303 (2006)
238. Spencer P E et al. *Phys. Rev. B* **71** 184310 (2005)
239. Kornilovitch P E, Alexandrov A S *Phys. Rev. B* **70** 224511 (2004)
240. Kornilovitch P E *Phys. Rev. B* **59** 13531 (1999)
241. Paci P et al. *Phys. Rev. Lett.* **94** 036406 (2005)
242. Seibold G, Grilli M *Phys. Rev. B* **72** 104519 (2005)
243. Kampf A P, Schrieffer J R *Phys. Rev. B* **42** 7967 (1990)
244. Andergassen S et al. *Phys. Rev. Lett.* **87** 056401 (2001)
245. Fratini S, Ciuchi S *Phys. Rev. B* **72** 235107 (2005)
246. Paci P et al. *Phys. Rev. B* **74** 205108 (2006)
247. Koikegami S, Aiura Y *Phys. Rev. B* **77** 184519 (2008)
248. Sawatzky G A *Nature* **342** 480 (1989)
249. Dessau D S et al. *Phys. Rev. Lett.* **81** 192 (1998)
250. Perfetti L et al. *Phys. Rev. Lett.* **87** 216404 (2001)
251. Perfetti L et al. *Phys. Rev. B* **66** 075107 (2002)
252. Schrupp D et al. *Europhys. Lett.* **70** 789 (2005)
253. Mahan G D *Many-Particle Physics* (New York: Kluwer Acad./ Plenum Publ., 2000)
254. Gerlach B, Löwen H *Rev. Mod. Phys.* **63** 63 (1991)
255. Röder H, Fehske H, Büttner H *Phys. Rev. B* **47** 12420 (1993)
256. Prelovšek P, Zeyher R, Horsch P *Phys. Rev. Lett.* **96** 086402 (2006)
257. Cataudella V et al. *J. Supercond. Novel Magn.* **22** 17 (2009)
258. Berciu M *Phys. Rev. Lett.* **97** 036402 (2006)
259. Goodvin G L, Berciu M, Sawatzky G A *Phys. Rev. B* **74** 245104 (2006)
260. Berciu M *Phys. Rev. Lett.* **98** 209702 (2007)
261. Berciu M, Goodvin G L *Phys. Rev. B* **76** 165109 (2007)
262. Covaci L, Berciu M *Europhys. Lett.* **80** 67001 (2007)
263. Covaci L, Berciu M *Phys. Rev. Lett.* **100** 256405 (2008)
264. Goodvin G L, Berciu M *Phys. Rev. B* **78** 235120 (2008)
265. Barišić O S *Phys. Rev. Lett.* **98** 209701 (2007)
266. Barišić O S *Phys. Rev. B* **76** 193106 (2007)
267. Freericks J K, Jarrell M, Scalapino D J *Phys. Rev. B* **48** 6302 (1993)
268. Cappelluti E, Ciuchi S *Phys. Rev. B* **66** 165102 (2002)
269. Cappelluti E, Ciuchi S, Fratini S *Phys. Rev. B* **76** 125111 (2007)
270. Cini M, D'Andrea A *J. Phys. C* **21** 193 (1988)
271. Ciuchi S et al. *Phys. Rev. B* **56** 4494 (1997)
272. Millis A J, Mueller R, Shraiman B I *Phys. Rev. B* **54** 5389 (1996)
273. Benedetti P, Zeyher R *Phys. Rev. B* **58** 14320 (1998)
274. Meyer D, Hewson A C, Bulla R *Phys. Rev. Lett.* **89** 196401 (2002)
275. Han J E, Gunnarsson O, Crespi V H *Phys. Rev. Lett.* **90** 167006 (2003)
276. Capone M, Ciuchi S *Phys. Rev. Lett.* **91** 186405 (2003)
277. Capone M, Carta P, Ciuchi S *Phys. Rev. B* **74** 045106 (2006)
278. Barentzen H *Phys. Rev. B* **53** 5598 (1996)
279. Yunoki S, Macridin A, Sawatzky G, Private communication (unpublished)
280. Pothuizen J J M, PhD Thesis (Groningen: Rijksuniversiteit, 1998)
281. Kim C, Private communication (unpublished)
282. Liu Z, Manousakis E *Phys. Rev. B* **51** 3156 (1995)
283. Alexandrov A S, Reynolds K *Phys. Rev. B* **76** 132506 (2007)
284. Liang R, Bonn D A, Hardy W N *Phys. Rev. B* **73** 180505(R) (2006)
285. Mishchenko A S et al., unpublished
286. De Filippis G, Cataudella V, Iadonisi G *Eur. Phys. J. B* **8** 339 (1999)
287. Lorenzana J *Europhys. Lett.* **53** 532 (2001)
288. Tempere J, Devreese J T *Eur. Phys. J. B* **20** 27 (2001)
289. Tempere J, Devreese J T *Phys. Rev. B* **64** 104504 (2001)
290. Cappelluti E, Ciuchi S, Fratini S *Phys. Rev. B* **79** 012502 (2009)
291. Johnson P D et al. *Phys. Rev. Lett.* **87** 177007 (2001)
292. Mihailović D et al. *Phys. Rev. B* **42** 7989 (1990)
293. Bi X-X, Eklund P C *Phys. Rev. Lett.* **70** 2625 (1993)
294. Alexandrov A S, Mott N *Polarons & Bipolarons* (Singapore: World Scientific, 1995)
295. Devreese J T, Tempere J *Solid State Commun.* **106** 309 (1998)
296. Devreese J T *J. Phys. Condens. Matter* **19** 255201 (2007)
297. Myasnikova A E, Myasnikov E N *Phys. Rev. B* **77** 165136 (2008)
298. Mishchenko A S, unpublished
299. Myasnikov E N, Myasnikova A E, Mastropas Z P *Zh. Eksp. Teor. Fiz.* **129** 548 (2006) [*JETP* **102** 480 (2006)]
300. Myasnikov É N, Myasnikova A É, Mastropas Z P *Fiz. Tverd. Tela* **48** 984 (2006) [*Phys. Solid State* **48** 1046 (2006)]
301. Vidmar L, Bonča J, Maekawa S *Phys. Rev. B* **79** 125120 (2009)
302. De Filippis G et al. *Phys. Rev. B* **80** 195104 (2009)
303. Schlesinger Z et al. *Phys. Rev. Lett.* **65** 801 (1990)
304. Valla T et al. *Science* **285** 2110 (1999)
305. Kaminski A et al. *Phys. Rev. Lett.* **84** 1788 (2000)
306. Bogdanov P V et al. *Phys. Rev. Lett.* **85** 2581 (2000)
307. Kaminski A et al. *Phys. Rev. Lett.* **86** 1070 (2001)
308. Gromko A D et al. *Phys. Rev. B* **68** 174520 (2003)
309. Sato T et al. *Phys. Rev. Lett.* **91** 157003 (2003)
310. Norman M R et al. *Phys. Rev. Lett.* **79** 3506 (1997)
311. Kim T K et al. *Phys. Rev. Lett.* **91** 167002 (2003)
312. Zeyher R, Greco A *Phys. Rev. B* **64** 140510 (2001)
313. Norman M R, Ding H *Phys. Rev. B* **57** R11089 (1998)
314. Eschrig M, Norman M R *Phys. Rev. Lett.* **85** 3261 (2000)
315. Manske D, Eremin I, Bennemann K H *Phys. Rev. Lett.* **87** 177005 (2001)
316. Eschrig M, Norman M R *Phys. Rev. Lett.* **89** 277005 (2002)
317. Manske D, Eremin I, Bennemann K H *Phys. Rev. B* **67** 134520 (2003)
318. Chubukov A V, Norman M R *Phys. Rev. B* **70** 174505 (2004)
319. Manske D *Theory of Unconventional Superconductors*: *Cooper-Pairing Mediated by Spin Excitations* (Heidelberg: Springer, 2004)
320. Fong H F et al. *Nature* **398** 588 (1999)
321. Mook H A et al. *Phys. Rev. Lett.* **70** 3490 (1993)
322. Fong H F et al. *Phys. Rev. Lett.* **75** 316 (1995)
323. Vignolle B et al. *Nature Phys.* **3** 163 (2007)
324. Sandvik A W, Scalapino D J, Bickers N E *Phys. Rev. B* **69** 094523 (2004)
325. Dai P et al. *Science* **284** 1344 (1999)
326. Wilson S D et al. *Nature* **442** 59 (2006)
327. Zhao J et al. *Phys. Rev. Lett.* **99** 017001 (2007)
328. Macridin A et al. *Phys. Rev. Lett.* **97** 056402 (2006)
329. Cataudella V et al. *Phys. Rev. B* **70** 193105 (2004)
330. De Filippis G et al. *Phys. Rev. B* **72** 014307 (2005)
331. Ramšak A, Horsch P *Phys. Rev. B* **48** 10559 (1993)
332. Brinkman W F, Rice T M *Phys. Rev. B* **2** 1324 (1970)
333. Fujimori A et al. *J. Phys. Chem. Solids* **57** 1379 (1996)
334. Perroni C A, Cataudella V, De Filippis G *J. Phys. Condens. Matter* **16** 1593 (2004)
335. Berciu M, Sawatzky G A *Europhys. Lett.* **81** 57008 (2008)
336. Bonča J, Trugman S A *Phys. Rev. B* **64** 094507 (2001)
337. Alexandrov A S *Phys. Rev. B* **53** 2863 (1996)
338. Alexandrov A S, Kornilovitch P E *J. Phys. Condens. Matter* **14** 5337 (2002)
339. Hague J P et al. *Phys. Rev. Lett.* **98** 037002 (2007)
340. Fehske H, Loos J, Wellein G *Phys. Rev. B* **61** 8016 (2000)
341. Sakai T, Poilblanc D, Scalapino D J *Phys. Rev. B* **55** 8445 (1997)
342. Slezak C et al. *Phys. Rev. B* **73** 205122 (2006)
343. Rösch O, Gunnarsson O *Phys. Rev. Lett.* **93** 237001 (2004)
344. Rösch O, Sangiovanni G, Gunnarsson O *Phys. Rev. B* **75** 035119 (2007)
345. Capone M et al. *Phys. Rev. Lett.* **92** 106401 (2004)
346. Sangiovanni G et al. *Phys. Rev. Lett.* **94** 026401 (2005)
347. Sangiovanni G, Capone M, Castellani C *Phys. Rev. B* **73** 165123 (2006)
348. Zhong J, Schüttler H-B *Phys. Rev. Lett.* **69** 1600 (1992)
349. Fehske H et al. *Phys. Rev. B* **51** 16582 (1995)
350. Wellein G, Röder H, Fehske H *Phys. Rev. B* **53** 9666 (1996)
351. Matsueda H, Tohyama T, Maekawa S *Phys. Rev. B* **74** 241103(R) (2006)
352. Matsueda H et al. *Phys. Rev. B* **77** 193112 (2008)
353. Hanaguri T et al. *Nature* **430** 1001 (2004)
354. Kohsaka Y et al. *Science* **315** 1380 (2007)
355. Pan S H et al. *Nature* **413** 282 (2001)
356. Singer P M, Hunt A W, Imai T *Phys. Rev. Lett.* **88** 047602 (2002)
357. Pavlenko N, Kopp T *J. Phys. Condens. Matter* **20** 395203 (2008)
358. Hague J P, Kornilovitch P E, Alexandrov A S *Phys. Rev. B* **78** 092302 (2008)
359. Berciu M, Mishchenko A S, Nagaosa N, arXiv:0906.1233
360. Pavlenko N, Kopp T *Phys. Rev. Lett.* **97** 187001 (2006)